

1 **Title:** Perturbation increases source-dependent organic matter degradation rates in estuarine
2 sediments.

3

4 **Author information**

5 Guangnan Wu¹, Klaas G.J. Nierop², Bingjie Yang³, Stefan Schouten³, Gert-Jan Reichart^{1, 2}, Peter
6 Kraal¹

7

8 ¹ Royal Netherlands Institute for Sea Research, Department of Ocean Systems, Landsdiep 4, 1797
9 SZ 't Horntje, The Netherlands

10 ² Utrecht University, Faculty of Geosciences, Princetonlaan 8a, 3584 CB Utrecht, The Netherlands

11 ³ Royal Netherlands Institute for Sea Research, Department of Marine Microbiology &
12 Biogeochemistry, Landsdiep 4, 1797 SZ 't Horntje, The Netherlands

13

14 **Corresponding author**

15 Guangnan Wu (guangnan.wu@nioz.nl)

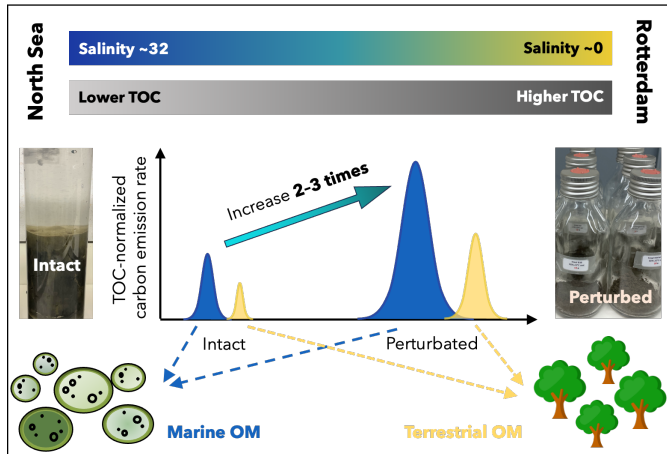
16

17

18 **Abstract**

19 Despite a relatively small surface area on Earth, estuaries play a disproportionately important role in
20 the global carbon cycle due to their relatively high primary production and rapid organic carbon
21 processing. Estuarine sediments are highly efficient in preserving organic carbon and thus often rich
22 in organic matter (OM), highlighting them as important reservoirs of global blue carbon. Currently,
23 estuaries are facing intensified human disturbance, one of which is sediment dredging. To understand
24 estuarine carbon dynamics and the impact of perturbations, insights into sediment OM sources,
25 composition, and degradability are required. We characterized the sediment OM properties and
26 oxidation rates in one of the world's largest ports, the Port of Rotterdam, located in a major European
27 estuary. Using a combination of OM source proxies and end-member modeling analysis, we
28 quantified the contributions of marine (10–65%), riverine (10–60%), and terrestrial (10–65%) OM
29 inputs across the investigated transect, with salinity ranging from 32 (marine) to almost 0 (riverine).
30 Incubating intact sediment cores from two contrasting sites (marine versus riverine) suggested that
31 OM degradation rates in marine sediments were about four times higher than those in riverine
32 sediments, which was also observed during a 35-day subaerial bottle incubation experiment with
33 mixed surface sediment. Moreover, subaerial incubation of mixed sediment showed a two- to three-
34 fold increase in OM degradation rates compared to intact core incubation, highlighting that
35 perturbation and subsequent enhanced oxygen availability can substantially boost OM degradation.
36 By combining detailed quantitative characterization of estuarine OM properties with degradation
37 experiments under varying conditions, the results further our understanding of the factors that govern
38 OM degradation rates in (perturbed) estuarine systems. Ultimately, this contributes to constraining the
39 impact of human perturbation on OM cycling in estuaries and its role in the carbon cycle.
40

41 **Graphical abstract**



42
43
44

45 **1. Introduction**

46 Estuaries are highly dynamic aquatic systems that are influenced by simultaneous marine, riverine,
47 and terrestrial inputs. In this transition zone, strong and variable gradients exist in hydrodynamic and
48 sediment properties, resulting in dynamic and complex cycles of key elements such as carbon
49 through coupled physical, chemical, and biological processes (Barbier et al., 2011; Dürr et al., 2011;
50 Laruelle et al., 2010). Despite representing only 0.03% of the surface area of marine systems,
51 estuaries are estimated to release approximately 0.25 Pg carbon annually into atmosphere on a
52 global scale, which is equivalent to 17% of the air-water CO₂ gas exchange of the entire open ocean
53 (Bauer et al., 2013; Li et al., 2023). Additionally, estuarine sediments store large amounts of organic
54 carbon (Macreadie et al., 2019; McLeod et al., 2011); due to high productivity and high sedimentation
55 rates, carbon burial rates in estuaries are up to one order of magnitude higher than forest soils and
56 three orders of magnitude higher than in open ocean sediments (Kuwae et al., 2016). Their
57 disproportionately large importance in the global carbon cycle highlights the need to improve our
58 understanding of carbon dynamics in estuarine systems.

59

60 Organic matter (OM), a fundamental component of sediment, plays a key role in sediment carbon
61 fluxes and sequestration. Degradation of OM contributes to the release of carbon dioxide (CO₂) and
62 methane (CH₄). This is a dynamic process that proceeds through a series of enzymatic reactions
63 involving different organisms, oxidants, and intermediate compounds. Studies have pointed out the
64 importance of OM characteristics in influencing the rate and extent of OM degradation (Burd et al.,
65 2016; Burdige, 2007; LaRowe and Van Cappellen, 2011). For instance, extensively degraded OM and
66 biopolymers such as cellulose and lignin are less susceptible to degradation than freshly produced
67 nitrogenous compounds (Arndt et al., 2013). Estuarine systems have diverse terrestrial and aquatic
68 OM sources, exhibiting varying degrees of degradability (Canuel and Hardison, 2016). Moreover,
69 interactions between OM and other components (organic or inorganic) during transportation,
70 deposition, and mineralization can alter OM characteristics. Processes such as condensation,
71 (geo)polymerization and mineral association increase OM resistance to degradation, thereby
72 promoting OM preservation (Wakeham and Canuel, 2006).

73

74 Sediment OM degradation is also influenced by ambient conditions at the sediment-water interface
75 and in the sediment (Arndt et al., 2013; Burd et al., 2016; Burdige, 2007; LaRowe and Van Cappellen,
76 2011). The degradation pathway follows the sequential utilization of the terminal electron acceptors
77 (TEAs), typically in the order of O₂, NO₃⁻/NO₂⁻, Mn (IV), Fe (III) and SO₄²⁻, with a progressive
78 decrease in energy yield down the redox ladder. The availability of these TEAs is greatly influenced by
79 the depositional environment. Estuaries are highly dynamic systems with strong and shifting salinity
80 (i.e. sulfate) gradients exist. This results in strong spatial variability in OM degradation pathways and
81 carbon dynamics (Cao et al., 2021). Specifically, large fluctuations in salinity and thus sulfate (SO₄²⁻)
82 availability between sites will affect CH₄ emissions because sulfate-driven methane oxidation provides
83 a highly effective CH₄ filter in surface sediments (e.g. Egger et al., 2018; Lovley and Phillips, 1986).
84 Moreover, compilation of field data reveals that organic carbon burial efficiency varies substantially in

space because the availability and exposure time of TEAs are influenced by environmental factors such as sedimentation rate (Arndt et al., 2013; Freitas et al., 2021). Estuaries are often characterized by relatively high sedimentation rates, with supply of riverine material that settles under low flow velocities at the river mouths as well as large inputs of (re)suspended marine matter from the coastal zone (Hutchings et al., 2020). Oxygen transport into the sediment is sufficiently low relative to the flux of reactive organic carbon to these sediments to maintain very shallow oxygen penetration depths, on the scale of micro- to millimeters (Burdige, 2012). By notably reintroducing O₂ to OM previously buried in oxygen-limited environments, sediment disturbance caused by natural processes (e.g. storm-induced mixing events, bioturbation) and human activities (e.g. dredging, bottom trawling) can change sediment redox chemistry and thereby have a profound effect on OM degradation pathways and burial efficiency (Aller, 1994).

96

97 Although estuaries have been widely studied from an ecological perspective, large variation in OM
98 properties and cycling processes within and across estuarine systems contributes to the uncertainty in
99 quantifying their significance in the global carbon cycle. This uncertainty is partially due to the highly
100 diverse OM sources and properties in estuarine systems. Many studies of estuarine OM sources use
101 bulk proxies such as the weight ratio of total organic carbon to total nitrogen (C/N ratio) and their
102 stable isotope ratios ($\delta^{13}\text{C}_{\text{org}}$ and $\delta^{15}\text{N}$; Canuel and Hardison, 2016; Carneiro et al., 2021; Cloern et
103 al., 2002; Middelburg and Nieuwenhuize, 1998). In other studies, OM sources have been investigated
104 by identifying biomarker compounds associated with specific sources and transformation processes.
105 For example, the branched and isoprenoid tetraether (BIT) index, based on the relative abundance of
106 terrestrially and/or freshwater-derived branched glycerol dialkyl glycerol tetraether (GDGT) versus
107 marine-derived isoprenoid GDGT crenarchaeol, was adopted to quantify the relative contribution of
108 terrestrial OM in sediments (Herfort et al., 2006; Hopmans et al., 2004; Smith et al., 2010; Strong et
109 al., 2012). Some studies focused on macromolecular organic matter (MOM) composition in sediments
110 to identify OM sources (Kaal et al., 2020; Nierop et al., 2017). Lignin, an important constituent of
111 vascular plant MOM, has proved to be a useful tracer of vascular plant inputs to estuarine/coastal
112 margin sediment (Bianchi and Bauer, 2012; Buurman et al., 2006; Fabbri et al., 2005; Hedges and
113 Oades, 1997; Kaal, 2019). Furthermore, the relationship between OM source and degradability can
114 be intricate, which inhibits the quantitative understanding of estuarine OM degradation.

115

116 Understanding the processing of OM within estuaries takes on further importance because many
117 estuarine systems are intensively altered by human activities (Arndt et al., 2013; Heckbert et al.,
118 2012; Holligan and Reiners, 1992). To increase or maintain waterway navigability, dredging is
119 commonly practiced in many coastal regions and rivers worldwide. More than 600 million m³ of
120 dredged material is generated annually just in Western Europe, China, and the USA (Amar et al.,
121 2021). While the dredged sediments are often treated as waste and disposed of at sea, there is a
122 growing trend of reusing dredged sediments on land, for instance in beach nourishment, habitat
123 restoration, and land reclamation (Brils et al., 2014). However, this impacts organic matter
124 degradation and subsequent CO₂ release from dredged materials in currently poorly understood

125 ways, with oxygen exposure potentially leading to enhanced carbon remineralization (LaRowe et al.,
126 2020). Given the need for sediment dredging and sustainable management of these materials (van de
127 Velde et al., 2018), it is of great importance to understand to what extent anthropogenic sediment
128 perturbations affect OM processing in and carbon emissions from estuarine sediments.

129

130 In this study, we investigate the spatial variability in OM content and properties and relationships
131 between OM source, composition, and degradability along a salinity gradient in the profoundly
132 disturbed Port of Rotterdam estuarine environment of the Rhine-Meuse delta system. Given the
133 frequent dredging activities in the study area, which hosts a globally major port, we aim to understand
134 the impact of sediment dredging and its potential land applications on carbon dynamics. We used a
135 combination of bulk OM proxies, BIT index, macromolecular organic matter (MOM) composition
136 analysis, as well as end-member modelling to understand OM sources and composition. Furthermore,
137 organic matter degradation rates were estimated both in 8-h sediment core incubation (mimicking in
138 situ condition) and 37-day bottle incubations with mixed surface sediments under atmospheric
139 conditions (representing subaerial application of dredged sediment). This study shows that variability
140 in OM sources and subsequently molecular properties, as well as perturbation (i.e. introduction of
141 oxygen), have important effects on OM degradation rates, providing important implications for
142 estuarine sediment management strategies.

143

144 **2. Materials and methods**

145 **2.1. Study area and sample collection**

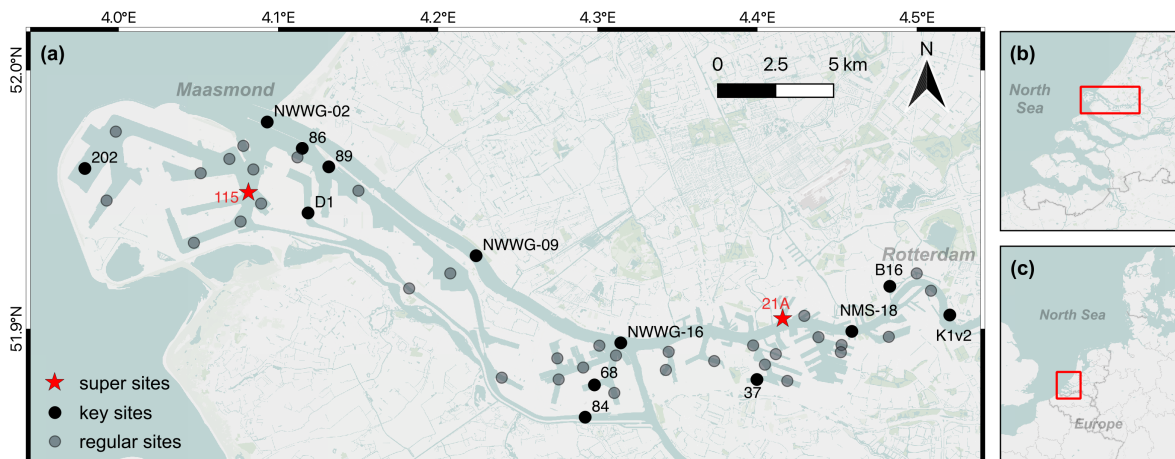
146 The study area is located in the northern part of the Rhine-Meuse estuary (Fig. 1), spanning from
147 Rotterdam city to the Maasmond. This area representing a transitional environment from riverine to
148 marine is heavily urbanized and hosts one of the world's largest ports, the Port of Rotterdam (PoR).
149 Every year, large amounts of sediment are deposited in the harbor from both rivers as well as the
150 North Sea (Kirichek et al., 2018). The water channel maintenance and harbor expansion lead to an
151 increasing need for sediment dredging throughout the PoR. Due to higher sedimentation rates and
152 the demand for deeper navigation channels at the river mouth, dredging is more frequently performed
153 in the western (marine) part (e.g. site 115) than in the eastern (riverine) part (e.g. 21A; Kirichek et al.,
154 2018). Currently, over 10 million m³ of dredged materials are generated from the PoR annually, most
155 sediments (classified as clean) being relocated to the shallow North Sea, while approximately 10%
156 (classified as contaminated) being stored subaerially in a holding basin in the PoR area (Kirichek et
157 al., 2018).

158

159 Bulk sediments were collected from 49 selected locations throughout the study area in the summer of
160 2021. These sites were selected from over 300 monitoring sites in the Port of Rotterdam to represent
161 the full spectrum of depositional conditions in the main waterway and adjacent harbor areas from
162 marine to riverine (Fig. 1). One sediment core from each site was collected using a gravity corer (ø9
163 cm). Once on deck, materials in the corer (down to ~50 cm depth) were emptied into 5-L
164 polypropylene buckets that were closed and stored in the fridge at 4 °C. These samples, later referred

165 as bulk sediments, were further processed within a week after collection at the Royal Netherlands
166 Institute for Sea Research (NIOZ) on Texel, the Netherlands. In addition to bulk sediments, intact
167 sediment cores were collected in summer 2022 upon revisiting two strongly contrasting sites (referred
168 as 'super sites' in Fig. 1) representing marine (site 115, salinity 29) and riverine (site 21A, salinity 5)
169 end-members in the PoR area. The intact sediment cores were immediately cooled, transported back
170 to the NIOZ and used in whole-core incubation experiments (see section 2.5) within 5 hours after
171 collection.

172



173
174 **Fig. 1.** (a) The investigated study area and sampling sites. Sediments from all 49 sites were subjected
175 to bulk analyses (e.g. grain size, TOC, TN) as detailed in section 2.2. Sediments from 13 key sites
176 were used for lipid and MOM analysis as detailed in section 2.3 and 2.4, respectively. Sediment cores
177 from two super sites were used in a whole-core incubation experiment as detailed in section 2.5. (b)
178 The location of investigated study area in the Rhine–Meuse estuary. (c) The location of Rhine-Meuse
179 estuary in Western Europe. Map created using QGIS software. Basemap courtesy of Mapbox.
180

181 2.2. Sample processing and analysis

182 Bulk sediments from each of the 49 sites were thoroughly mixed using a spatula in the buckets.
183 Approximately 40 mL of wet sediment were transferred into 50-mL polypropylene centrifuge tubes
184 (Falcon) and centrifuged at 3000 rpm for 20 min (Hermle Z 446). In a N₂-purged glove bag, the
185 porewater was immediately filtered through a 0.45-μm nylon syringe filter (MDI). Salinity was
186 estimated by comparing the porewater sodium (Na) concentration to the average seawater sodium
187 concentration and salinity in the North Sea (IJsseldijk et al., 2015; Steele et al., 2010). For Na
188 analysis, the porewater was diluted around 900 times in 1 M double-distilled HNO₃ and analyzed by
189 inductively coupled plasma mass spectrometry (ICP-MS, Thermo Scientific, Element 2).

190

191 The centrifuge tubes with wet sediment residues after centrifugation were purged with N₂ and stored
192 at -20 °C in N₂-purged, gas-tight Al-laminate bags to prevent oxidation. To prepare for subsampling,
193 the sediment residues were thawed overnight in a N₂-purged glove bag (Coy Laboratories) and
194 subsequently homogenized. One portion of wet sediment residue (~1 g) was mixed with 50 mL of 3 g

195 L⁻¹ sodium pyrophosphate solution and gently shaken to disaggregate particles. Particle size
196 distribution was determined using a Coulter laser particle sizer (Beckman Coulter), from which
197 percentages of clay (0–2 µm), silt (2–63 µm), sand (63–2000 µm) and the median particle size (D50)
198 were calculated.

199

200 Approximately 10 g of wet sediment residue was freeze-dried (Hetrosicc freeze dryer) for 72 h and
201 manually ground with an agate pestle and mortar, and further subsampled for carbon and nitrogen
202 (CN) analysis. One subsample of the freeze-dried sediment (~10 mg) was directly used for measuring
203 total nitrogen (TN) and stable nitrogen isotope composition (expressed as $\delta^{15}\text{N}$, relative to
204 atmospheric nitrogen) by a CN elementary analyzer (Thermo Scientific, FLASH 2000) coupled to a
205 Delta V Advantage isotope ratio mass spectrometer (Thermo Scientific). Another freeze-dried
206 subsample (~0.5 g), firstly treated with 1 M HCl to remove carbonates, was used for measuring total
207 organic carbon (TOC) and stable carbon isotope composition (expressed as $\delta^{13}\text{C}_{\text{org}}$, relative to Vienna
208 Pee Dee Belemnite). Certified laboratory standards (acetanilide, urea, and casein) were used for
209 calibration with each sample. Precision and accuracy for standards and triplicate samples were
210 $\pm 0.3\%$ for $\delta^{13}\text{C}_{\text{org}}$ and $\delta^{15}\text{N}$, and the relative standard deviation (RSD; standard deviation/mean) was
211 <10% for TOC and TN.

212

213 **2.3. Lipid extraction and analysis**

214 Sediments from 13 key locations (Fig. 1), selected to cover the full river-marine salinity transect, were
215 used for lipid and MOM analyses. Freeze-dried and homogenized sediments (2–10 g) were
216 ultrasonically extracted with dichloromethane (DCM):methanol (2:1, v:v) five times. For each sample,
217 extracts obtained from the five steps were combined. The total extract was separated over an Al₂O₃
218 column into an apolar, neutral and polar fraction using hexane:DCM (9:1, v:v), hexane:DCM (1:1, v:v)
219 and DCM:methanol (1:1, v:v), respectively. The polar fractions containing glycerol dialkyl glycerol
220 tetraethers (GDGTs) were dried under N₂, dissolved in hexane:propanol (99:1, v:v), and filtered using
221 a 0.45 µm PTFE filter. This fraction was subsequently analyzed with ultra-high performance liquid
222 chromatography mass spectrometry (UHPLC-MS) on an Agilent 1260 Infinity HPLC coupled to an
223 Agilent 613MSD according to (Hopmans et al., 2016). The isoprenoid and branched GDGTs were
224 detected by scanning for their [M+H]⁺ ions. The BIT index was calculated according to (Hopmans et
225 al., 2004).

226

227 **2.4. Macromolecular organic matter (MOM) isolation and analysis**

228 The sediment residues, remaining after lipid extraction, from the 13 samples from key locations were
229 dried under N₂. To isolate MOM, dried sediment residue (2–3 g) was transferred into 50-mL centrifuge
230 tubes and decalcified with 30 mL 1 M HCl for 4 h, later rinsed twice with 25 mL milli-Q water (18 MΩ).
231 After centrifugation and decanting the supernatant, 15-mL 40% HF (analytical grade, Merck) was
232 added and shaken for 2 h at 100 rpm. The solution was diluted with milli-Q water to 50 mL and left
233 standing overnight, after which the solution was decanted to a high-density polyethylene plastic
234 container designated for HF waste. A volume of 15 mL 30% HCl was added and subsequently diluted

235 with milli-Q water to 50 mL. After shaking for 1 h and centrifugation, the solution was decanted, and
236 the residues were washed with milli-Q water three times to neutralize pH and subsequently freeze-
237 dried. The supernatant of all steps was collected in the HF waste container. Samples were
238 desulfurized using activated copper pellets in DCM. Suspensions were stirred overnight after which
239 the copper pellets and DCM were removed. The sample residue, containing the macromolecular
240 organic matter (MOM), was air-dried prior to the analysis.

241

242 The analysis of MOM was conducted at Utrecht University using the pyrolysis-gas chromatograph-
243 mass spectrometry method previously described in (Nierop et al., 2017). In short, the isolated MOM
244 was pyrolyzed on a Horizon Instruments Curie-Point pyrolysis unit. The pyrolysis unit was connected
245 to a Carlo Erba GC8060 gas chromatograph and the products were separated by a fused silica
246 column (CP-Sil5, 25 m, 0.32 mm i.d.) coated with CP-Sil5 (film thickness 0.40 μ m). The column was
247 coupled to a Fisons MD800 mass spectrometer. Pyrolysis products were identified using a NIST
248 library or by interpretation of the spectra, by their retention times and/or by comparison with literature
249 data. Quantification was performed according to (Nierop et al., 2017).

250

251 **2.5. Whole-core sediment incubation**

252 Triplicate intact sediment cores collected from two strongly contrasting sites (marine site 115 vs.
253 riverine site 21A) were used for whole-core incubation. These sites represent relatively intensively
254 dredged marine and riverine areas, respectively, that contribute significantly to the total annual
255 dredged sediment volume in the PoR. Prior to incubation, cores were carefully manipulated to have
256 ~15 cm of undisturbed top sediment (primary zone of diagenesis) with ~20 cm of overlying water
257 (achieving a ~ 1:1 water:sediment volume ratio which represents a balance between sensitivity in
258 measuring fluxes while avoiding excess accumulation of (inhibiting) reactants in the overlying water
259 and ensuring a small fraction of the overlying water is replaced by discrete sampling). After confirming
260 that the sediment surface was not disturbed, an oxygen sensor spot (Presens) was attached to the
261 inner wall of the core tube (5 cm from the top) to monitor O₂ in the overlying water. The cores, capped
262 at the bottom and open at the top, were submerged in bottom water from the corresponding site in an
263 incubation tank. Stirrers were placed in each core to mix the overlying water (at ~1 rpm) and the cores
264 were left open overnight to equilibrate. The water in the tank was kept fully oxygenated by sparging
265 with air using an aquarium pump. Temperature in the room was maintained at the measured in situ
266 bottom water temperature (19 °C). At the start of the incubation, the cores were capped with gas-tight
267 lids with an outlet to sample bottom water from the core and an inlet to replace sampled volume with
268 site water from a 20-L reservoir. Over the course of an eight-hour incubation period, 30 mL of bottom
269 water (equivalent to 2.3% of total overlaying water volume) were extracted at pre-determined time
270 intervals of 0, 1.5, 3.5, 5, 6.5, and 8 h. The dissolved O₂ concentration in the overlying water in each
271 core was measured every five minutes using the sensor spots and a Presens OXY-4 SMA meter with
272 fiber optic cables, operated using Presens Measurement Studio 2. Immediately after sampling, the
273 water samples were filtered using 0.45- μ m nylon syringe filters for dissolved inorganic carbon (DIC),

274 total alkalinity (TA) and dissolved inorganic nitrogen (DIN: NH_4^+ , NO_3^- , NO_2^-) analysis, while an
275 unfiltered subsample was retained for methane (CH_4) analysis.

276

277 The DIC samples were diluted 10 times in N_2 -purged 25 g L^{-1} sodium chloride solution without
278 headspace and analyzed within 24 hours on a continuous flow analyzer (QuAAstro, Seal Analytical).
279 The TA samples were kept at 5 °C without treatment and measured within a week using the same
280 analyzer. The DIN samples were stored at -20 °C and later analyzed on a TRAACS 800+ continuous
281 flow analyzer. For CH_4 , 12 mL of bottom water was directly transferred into a 12 mL Exetainer vial
282 (Labco), immediately poisoned with ~0.25 mL of saturated zinc chloride solution and capped with a
283 butyl rubber stopper ensuring no headspace was present. Dissolved CH_4 concentration was
284 determined using a headspace technique (Magen et al., 2014). Prior to the measurement, 1 mL of N_2
285 headspace was injected through the stopper in each Exetainer vial while a needle allowed the
286 equivalent volume of sample to escape, after which the samples were equilibrated for a week.
287 Headspace CH_4 concentrations were then measured on a gas chromatograph (Thermo Scientific
288 FOCUS GC) equipped with a HayeSep Q Packed GC Column and a flame ionization detector. A
289 calibration curve was made using a certified 1000 ppm CH_4 standard (Scott Specialty Gases
290 Netherlands B.V.). From the measured CH_4 concentration in the headspace, the total dissolved CH_4 in
291 the bottom water was calculated using the equations in (Magen et al., 2014) with the Bunsen
292 coefficient (Yamamoto et al., 1976). Benthic fluxes of DIC and CH_4 were calculated using the
293 concentration changes of solutes in the bottom water of closed cores during the incubation period, as
294 determined by linear regression analysis of the individual time series. Total organic matter
295 mineralization was partitioned into aerobic and anaerobic contributions. Assuming a 1:1 stoichiometric
296 relationship between O_2 consumption rate and DIC production rate for aerobic mineralization, the
297 aerobic fraction was calculated from measured O_2 consumption, and the remaining OM-derived DIC
298 production was attributed to anaerobic mineralization.

299

300 **2.6. Subaerial incubation of dredged sediment**

301 To investigate OM degradability under oxygen exposure during dredged sediment processing, open-
302 air bottle incubations were conducted in triplicate for six sediments from sites that covered contrasting
303 depositional and sedimentary conditions within the research area: three marine (115, 86, NWWG-02;
304 Fig. 1a) and three riverine (21A, B16, K1v2; Fig. 1a), with differing sediment texture (silt-rich and
305 sand-rich) in both groups. To obtain minimally altered sediment in which the water content could be
306 accurately and rapidly adjusted, and to ensure reproducibility, we used freeze-dried and homogenized
307 sediments from the six sites, in triplicate. The freeze-dried sediment was transferred into 330-mL
308 borosilicate glass bottles, resulting in a thin sediment layer (< 5 mm). Artificial rainwater (composition
309 in Table S1) was added to achieve a water content of 60% water-filled pore space (assuming the
310 same porosity after rewetting; calculation provided in the SI), which is a water content optimal for soil
311 respiration (Fairbairn et al., 2023). The rewetted sediments were incubated in the dark at room
312 temperature (20 °C). The CO_2 emission rates were measured on day 2, 6, 9, 16, 23, 30 and 37; in the
313 later stages in incubations, the rates declined significantly and became relatively stable after around

314 one-month incubation, and the experiment was terminated. On the day of measurement, bottles were
315 sealed with rubber stoppers tightened with aluminum crimp caps for approximately 3 hours. We
316 measured the CO₂ concentrations in the headspace immediately after the bottles were capped and
317 approximately 3 hours later. The CO₂ accumulation in the headspace of each bottle during these 3
318 hours was used to calculate a CO₂ emission rate. For the rest of the time, bottles were kept open to
319 the atmosphere. The moisture level was maintained once a week and varied by less than 10% from
320 the target value.

321

322 The CO₂ measurement for the subaerial incubation was conducted by withdrawing a volume of 150
323 μ L headspace gas using a 250- μ L glass, gas-tight syringe (Hamilton). The headspace sample was
324 immediately injected into a gas chromatograph (GC, Agilent, 8890 GC system) equipped with a
325 Jetanizer and a flame ionization detector. Gases were carried by helium and separated by a
326 Carboxen-1010 PLOT analytical column (Sigma-Aldrich). Calibration was conducted by using certified
327 reference CO₂ gas (Scott specialty gases, Air Liquide, Eindhoven, The Netherlands).

328

329 To determine the percentage of degraded TOC over time, we firstly calculated the cumulative amount
330 of CO₂ emission and then normalized it to the total amount of organic carbon in the incubated
331 sediments, calculated from the dry sediment mass and its TOC content. The cumulative CO₂ emission
332 was obtained by integrating the CO₂ emission rate over time. For days when CO₂ emission rates were
333 not measured, the rates were estimated using spline interpolation. The integration and normalization
334 were performed using the 'AUC' (area under curve) function in RStudio.

335

336 **2.7. End-member modelling of OM sources**

337 Contributions of three major OM end-members (marine, riverine, and terrestrial) to the 49 sediments
338 were quantified based on $\delta^{13}\text{C}_{\text{org}}$ and C/N ratio using a Bayesian mixing model, MixSIAR (Stock et al.,
339 2018). Anthropogenic OM such as petroleum and coal products were not considered as they typically
340 have a much higher C/N ratio (Tumuluru et al., 2012) compared to the investigated samples here
341 (mostly <20), thus suggesting a limited contribution. Input from industrial and chemical waste is
342 considered being minimal because >90% of sediment is regarded as clean/safe with organic
343 contaminants below their national intervention values (Kirichek et al., 2018). We did not include
344 sewage OM and agricultural wastes as separate end-members due to their high variability in $\delta^{13}\text{C}_{\text{org}}$
345 (−28‰–−23‰; Shao et al., 2019) and C/N ratio (Chow et al., 2020; Puyuelo et al., 2011; Szulc et al.,
346 2021), and values largely overlaps with those of the considered three end-members. The model
347 incorporates the common ranges of three OM end-members in coastal environments (Table 1) and
348 employs Markov Chain Monte Carlo (MCMC) simulation to sample from the posterior distribution. The
349 distribution provides estimates of the mean contribution with standard deviation. The model was run in
350 RStudio with package "MixSIAR" integrated into the JAGS program.

351

352 **Table 1.** Mean values and standard deviations of $\delta^{13}\text{C}_{\text{org}}$ and C/N ratio of three OM end-members
 353 used in the MixSIAR analysis. Values from literature (Bianchi and Bauer, 2012; Finlay and Kendall,
 354 2007; Lamb et al., 2006).

End-member	Typical OM	$\delta^{13}\text{C}_{\text{org}}$ (‰)	C/N
Marine OM end-member	Marine POC, algae, bacteria	-20±4	7±3
Riverine OM end-member	Freshwater POC, algae, bacteria	-29±4	7±3
Terrestrial OM end-member	Vegetation, soil OM, bacteria	-26.5±5.5	30±18

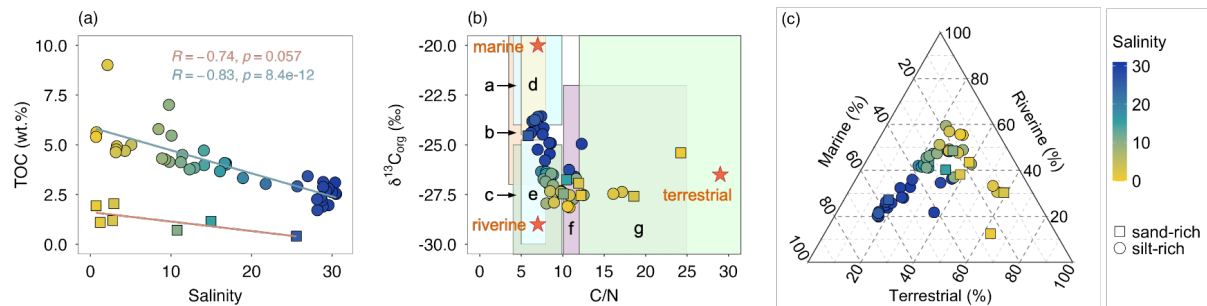
355

356 3. Results

357 3.1 Bulk geochemical feature of sediments

358 The PoR sediments were mostly (42 out of 49 samples) silt-rich with D50 smaller than 20 μm . A
 359 salinity gradient was observed in the study area increasing from approximately 0 at the most eastern
 360 part (Rotterdam city) to approximately 32 at the river mouth in the west. We observed a decrease in
 361 TOC content with increasing salinity (Fig. 2a). The silt-rich sediments generally contained more than
 362 2.5 wt.% TOC, with significantly lower TOC contents in the sand-rich sediments ($p < 0.01$, Student's t -
 363 test). The weight ratio of C/N was between 5 and 13 for most samples (45 out of 49), and the
 364 corresponding $\delta^{13}\text{C}_{\text{org}}$ was in the range of -29‰ to -23‰ (Fig. 2b). Despite a weak correlation
 365 between C/N ratio and $\delta^{13}\text{C}_{\text{org}}$ ($R = -0.38$, Pearson), both properties showed (moderately) strong
 366 trends against salinity (C/N ratio: $R = -0.66$; $\delta^{13}\text{C}_{\text{org}}$: $R = 0.68$, Pearson; Fig. 2b).

367



368

369 **Fig. 2.** Bulk geochemical properties of 49 sediment samples from the PoR. (a) TOC vs. salinity for
 370 both silt-rich ($\text{D50} < 20 \mu\text{m}$) and sand-rich ($\text{D50} > 50 \mu\text{m}$) sediments. (b) $\delta^{13}\text{C}_{\text{org}}$ and the weight ratio of
 371 C/N in sediments along salinity gradient in contrast to the typical $\delta^{13}\text{C}_{\text{org}}$ and C/N ranges for OM from
 372 coastal sediments in literature (Bianchi and Bauer, 2012; Finlay and Kendall, 2007; Lamb et al.,
 373 2006): **a** marine POC, **b** bacteria, **c** freshwater POC, **d** marine algae, **e** freshwater algae, **f** soil OM, **g**
 374 C_3 terrestrial plants. Orange star symbols represent the mean values of three OM sources used in
 375 end-member analysis. (c) The contributions (%) of marine, riverine and terrestrial OM using a mixing
 376 model. The standard deviation (10–25%) is provided in the Supplementary Information (SI, Table S2).

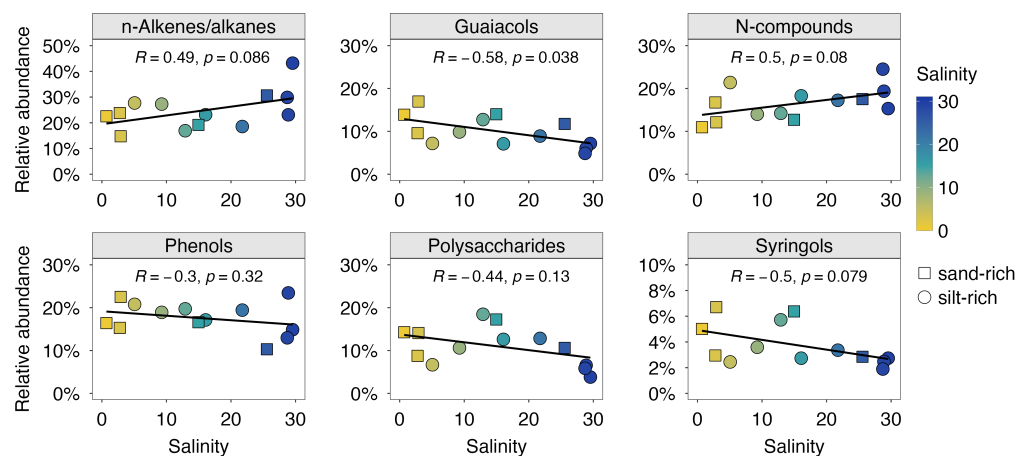
377

378 3.2. Flash pyrolysis products of MOM

379 Pyrolysis of isolated MOM produced hundreds of pyrolysis compounds. The identified pyrolysis
 380 products are listed in Supplementary Information (Table S3). They were divided into nine groups
 381 based on the chemical characteristics, following the approach detailed in Nierop et al. (2017). Here in

382 Fig. 3, we present the relative abundance of six MOM pyrolysate groups along the salinity gradient,
 383 including *n*-alkenes/alkanes, guaiacols, N-compounds, phenols, polysaccharide-derived products, and
 384 syringols. The other three groups: phytadienes and pris-1-ene were only minor constituents (relative
 385 abundance < 5%), and aromatics showed a negligible correlation with salinity ($-0.1 < R < 0.1$,
 386 Pearson; Fig. S1). With increasing salinity, we observed an increase in the relative abundance of *n*-
 387 alkenes/alkanes and N-compounds, while guaiacols, phenols, polysaccharides, and syringols
 388 decreased. The correlations were generally moderate or weak, as suggested by the magnitude of the
 389 correlation coefficient ($-0.6 < R < 0.6$, Pearson). Additionally, the correlation coefficients between the
 390 identified MOM pyrolysate groups and other bulk sediment properties (i.e. D50, C/N, $\delta^{13}\text{C}_{\text{org}}$) were
 391 also weak (see SI, Fig. S2).

392



393

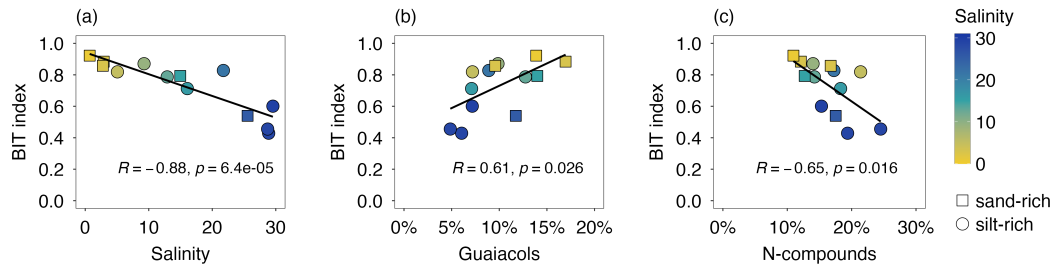
394 **Fig. 3.** The relative abundance of six groups of MOM pyrolysis products. Pearson correlation
 395 coefficient (R) measures the strength of the linear relationship between grouped pyrolysates and
 396 salinity.

397

398 **3.3. BIT index**

399 Crenarchaeol and branched GDGTs were detected in sediments from all 13 investigated sites. The
 400 calculated BIT index ranged between 0.43 and 0.92 (Fig. 4a). A strong negative correlation was
 401 observed between BIT index and salinity ($R = -0.88$, Pearson) and between BIT index and $\delta^{13}\text{C}_{\text{org}}$ (R
 402 = -0.83 , Pearson). In contrast, the correlations with MOM pyrolysate products were in general weak or
 403 moderate ($-0.6 < R < 0.6$, Pearson; Fig. S2), except for guaiacols and N-compounds (Fig. 4b & 4c).
 404 Additionally, we did not observe a significant difference between sand-rich and silt-rich sediments in
 405 BIT index values ($p > 0.5$, Student's t -test).

406



407

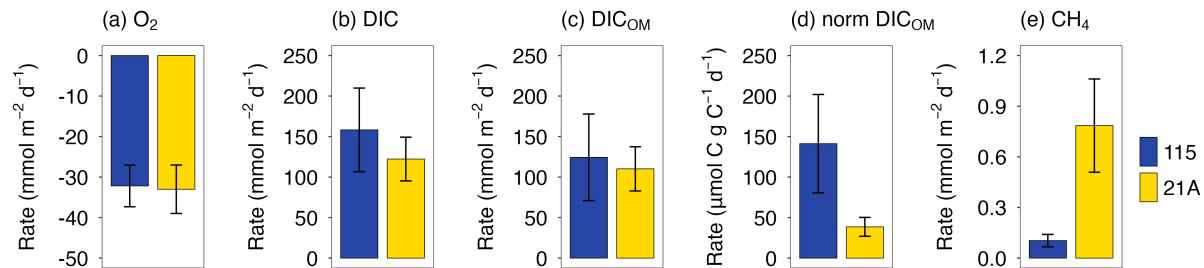
408 **Fig. 4.** The BIT index of 13 sediments against (a) salinity, (b) relative abundance of guaiacols, (c)
409 relative abundance of N-compounds.

410

411 3.4. Benthic fluxes on intact sediment cores

412 During the whole-core incubation, the O_2 concentration in the overlying water decreased linearly from
413 around 90% to 60% air-saturation for both the high salinity location (115, salinity 29, later referred as
414 'marine' location) and the low salinity location (21A, salinity 5, later referred as 'riverine' location; SI
415 Fig. S2). At the same time, concentrations of DIC and CH_4 in the overlying water increased linearly
416 with time (Fig. S3). Benthic O_2 consumption and DIC release rates showed no significant differences
417 between two contrasting locations ($p > 0.05$, Student's t -test), on average around 30 and 122–158
418 $mmol\ m^{-2}\ d^{-1}$, respectively (Fig. 5a, b). However, DIC was released into the overlying water at a much
419 higher rate, 4–5 times larger than O_2 consumption rate. Correcting the DIC flux for contributions not
420 associated with OM degradation (i.e. $CaCO_3$ dissolution) as described in the supplementary
421 information provided us with an estimate of the DIC flux from OM degradation (DIC_{OM}) which
422 accounted for 88–97% of the total DIC flux (Fig. 5c). When normalized to TOC to correct DIC_{OM} for
423 differences in bulk TOC content, the DIC flux at 115 was about four times higher than at site 21A (Fig.
424 5d). Additionally, the CH_4 efflux was one to two orders of magnitude smaller than the O_2 and DIC
425 fluxes and showed significant differences between two contrasting locations: the CH_4 efflux at the river
426 location was more than five times higher compared to the marine location (Fig. 5e).

427



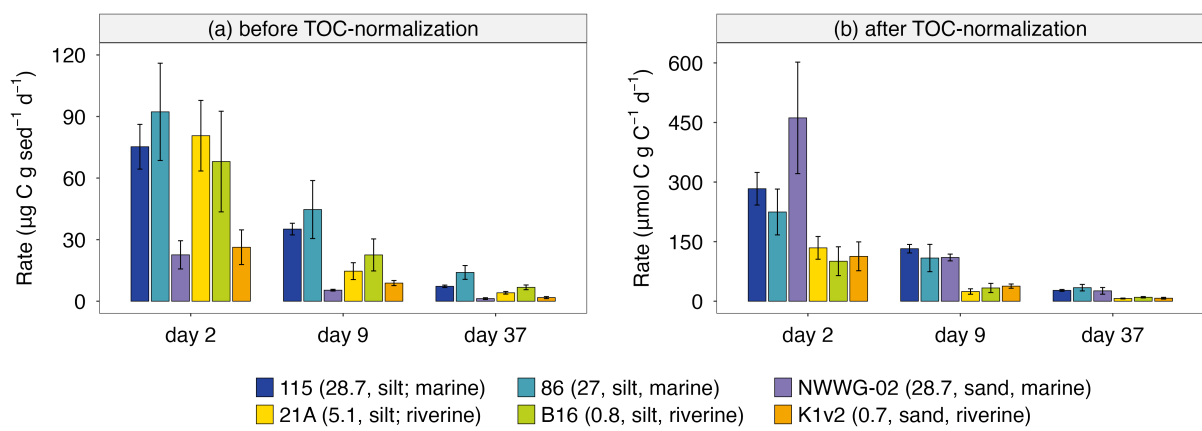
428

429 **Fig. 5.** Benthic fluxes of dissolved O_2 (a) and DIC (b) determined from whole-core incubation. Positive
430 and negative rates represent efflux (from sediment into overlying water) and influx (from overlying
431 water into sediment), respectively. The contribution of OM degradation to benthic DIC fluxes is shown
432 in panel (c) and further normalized by sediment TOC in panel (d). Panel (e) shows benthic CH_4 fluxes.
433 Error bars represent standard deviations from triplicate core incubations. Other measured fluxes (e.g.
434 DIN, total alkalinity) are available in Fig. S4.

435

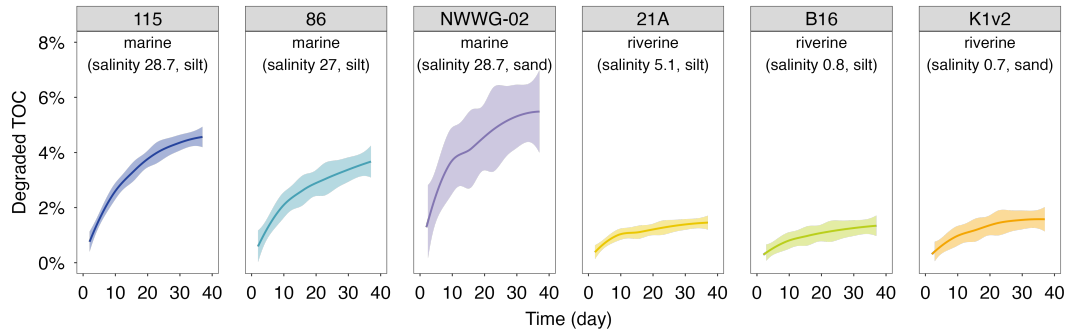
436 **3.5. Subaerial carbon emissions from bulk sediments**

437 During the aerobic incubation experiment, CO₂ accumulation was detected during the 3-hour rate
 438 measurements for all timesteps. The CO₂ emission rate, expressed as $\mu\text{g C g}^{-1} \text{ day}^{-1}$, was the
 439 highest at the start of the incubation. Rates dropped drastically in the first two weeks and then
 440 stabilized after day 25. Here we present carbon emission rates at three timesteps representing the
 441 initial stage, declining stage, and stable stage (Fig. 6). The silt-rich sediments showed both higher
 442 emission rates throughout the incubation period (up to 120 $\mu\text{g C g}^{-1} \text{ day}^{-1}$) and stronger decreases in
 443 rate over time (more than 60 $\mu\text{g C g}^{-1} \text{ day}^{-1}$), compared to sand-rich sediments (maximum rate
 444 around 35 $\mu\text{g C g}^{-1} \text{ day}^{-1}$; Fig. 6a). The TOC-normalized carbon emission rates were higher (up to
 445 three times) in the three marine sediments (salinity 27–28) compared to the three riverine sediments
 446 (salinity 0–5) throughout the experiment (Fig. 6b).



447
 448 **Fig. 6.** Carbon emission rates in aerobic incubation at day 2, day 9 and day 37 from six sediments.
 449 Note the different scales and units for the y-axis for carbon emission rates before TOC-normalization
 450 (a) and after TOC-normalization (b). Site information (i.e. salinity, sediment texture, and
 451 marine/riverine location within the PoR) is given in brackets in the legend.
 452

453 The decreasing trend of CO₂ emission rate was also reflected in the cumulative percentage of
 454 degraded TOC over time (Fig. 7), which increased fast initially and stabilized towards the end of the
 455 incubation experiment. After the 37-day incubation period, the amount of degraded TOC ranged from
 456 1 to 7% for the investigated sites. Additionally, the percentage of degraded TOC was 2–4 times higher
 457 in sediments from marine locations than those in river locations, consistent with the differences in
 458 carbon emission rates (Fig. 6b).
 459



460

461 **Fig. 7.** The percentage of degraded TOC over time in aerobic incubation experiments. The shading
 462 areas represent the 95% confidential interval for the fitted locally estimated scatterplot smoothing
 463 (LOESS) curves.

464

465 **4. Discussion**

466 **4.1 Organic matter content, source and composition in estuarine sediments**

467 The PoR sediments are characterized by relatively high TOC contents compared to the North Sea
 468 surface sediments (0.03–2.79 wt.%; Wiesner et al., 1990), but in the range of Dutch coastal
 469 sediments (0–9.8 wt.%; Stronkhorst and Van Hattum, 2003) or other harbor systems such as the Port
 470 of Hamburg (2–7.6 wt.%; Zander et al., 2020). The high carbon content arose from high productivity
 471 and rapid burial of OM under high sedimentation rates; oxygen penetration is limited in rapidly
 472 accumulating, organic-rich sediment, and thus most OM breakdown occurs via relatively slow,
 473 anaerobic processes (Schulz and Zabel, 2006). Moreover, the fine sediment texture observed at most
 474 investigated sites limits oxygen diffusion and provides more sorption surface for OM (Keil et al., 1994),
 475 both contributing to the preservation of sedimentary OM and thus high TOC content compared to
 476 sandy sediment. This is expressed in the relatively low TOC content (0–2.5 wt.%) of the coarser-
 477 grained sediments shown in Fig. 2a. Besides the clear impact of grain size on OM content, a general
 478 decreasing trend in sediment TOC contents from river to marine area of the PoR sediments was
 479 observed, in line with previous work on estuarine sediment OM (Strong et al., 2012). The relatively
 480 low OM content in sediment from the marine-dominated sites in part arises from the large input (up to
 481 5.7 million tons per year) in this area of repeatedly resuspended, OM-poor coastal sediment
 482 transported by strong tide and waves (Cox et al., 2021). More frequent dredging activities at the
 483 marine sites may also contribute to the lower OM content (Fig. 2a), as also witnessed in other coastal
 484 sediments (Aller et al., 1996). Furthermore, moving downstream from the riverine to the marine part of
 485 estuarine systems, the contribution of OM-rich riverine sediment not only decreases, but continuing
 486 OM degradation in this transported sediment further diminishes the amount of riverine OM (Bianchi et
 487 al., 2018; Freitas et al., 2021).

488

489 The OM burial and degradation are not only affected by the sediment dynamics as described above,
 490 but also by the source and inherent properties of the OM. The $\delta^{13}\text{C}_{\text{org}}$ and C/N ratio have been widely
 491 used to assess OM sources in coastal environments (Canuel and Hardison, 2016; Lamb et al., 2006;

492 Li et al., 2021; Middelburg and Nieuwenhuize, 1998). The OM in the estuarine ecosystems can
493 originate from multiple sources, and the typical ranges of $\delta^{13}\text{C}_{\text{org}}$ and C/N ratio for the common OM
494 sources are indicated in Fig. 2b. The trends in $\delta^{13}\text{C}_{\text{org}}$ and C/N ratio suggest that OM in the PoR
495 sediments is derived from a mixture of marine, riverine and terrestrial OM that are sourced from algae,
496 bacteria, soil OM, and terrestrial plants, the relative contribution of these sources being a function of
497 depositional conditions (riverine versus marine) also reflected by salinity (Fig. 2b). The observed
498 $\delta^{13}\text{C}_{\text{org}}$ values (−29–−23‰) and their trend against salinity are similar to those in the broader Rhine
499 estuary reported in earlier work by (Middelburg and Herman, 2007), suggesting that intense sediment
500 reworking in connection with harbor expansion over the last 15 years has had little impact on
501 sediment OM sources. Furthermore, the range in observed $\delta^{13}\text{C}_{\text{org}}$ values is lower than that reported
502 for temperate marine OM (−18 and −22‰; Thornton and McManus, 1994), reflecting a significant non-
503 marine OM source even under nearly marine conditions at the river mouth. Quantification of the
504 different sources using end-member modelling similarly indicates that the dominant OM source shifts
505 with depositional environment: terrestrial OM in the most river-dominated locations (up to 65%,
506 salinity < 5), freshwater OM in the river-sea transitional area (~ 45%, 5 < salinity < 25), and marine
507 OM in the river-mouth area (up to 65%, salinity > 25).

508

509 Regarding the range of and trend in C/N values, it is important to note that the value is subject to OM-
510 specific alterations during sediment diagenesis: for higher plant litter, the C/N ratio decreases during
511 decomposition, while for aquatic detritus the C/N ratio increases during degradation (Hedges and
512 Oades, 1997; Wakeham and Canuel, 2006). These opposing diagenetic trajectories can result in a
513 convergence of C/N ratios of terrestrial and aquatic detritus (Middelburg and Herman, 2007). This
514 may explain the observation that bulk sediments at many of the investigated sites in the PoR research
515 area have C/N ratios near the upper limit of the typical range for freshwater algae (~8) or POC (~10),
516 or around the lower limit of the typical range for C₃ plants (~12, Fig. 2b). Compared to the C/N ratio,
517 the BIT index is thought to be less sensitive to diagenetic effects (Hopmans et al., 2004). This proxy
518 indicates a predominant riverine and/or terrestrial source of the sedimentary OM (Schouten et al.,
519 2013). The BIT values from this study are in line with the values previously determined by Herfort et
520 al. (2006) in sediment at Maassluis (0.74–0.82; close to NWWG-09, Fig 1), while they are much
521 higher than those determined in coastal sediments of the southern North Sea (0.02–0.25; Herfort et
522 al., 2006), highlighting the sharp transition in OM composition between estuarine and coastal systems
523 and the importance of non-marine OM throughout the harbor system.

524

525 The source proxies presented above ($\delta^{13}\text{C}_{\text{org}}$, C/N, BIT) indicate a strong terrestrial and riverine OM
526 signature across the salinity gradient in the PoR study area, with a considerable marine contribution
527 at the river mouth. The pyrolysis products from MOM offer additional insights into sediment OM
528 sources and composition. Guaiacols and syringols are pyrolytic markers of terrestrial OM, as they are
529 characteristic structural moieties of lignin, a typical biopolymer of higher plants. Their relative
530 abundance together (7–28%) falls within the reported lignin fractions (3–57%) for various coastal
531 aquatic environments (Brandini et al., 2022; Burdige, 2007; Kaal et al., 2020). Although having

532 multiple potential sources, the markers of polysaccharides in the investigated samples showed strong
533 positive correlations with both guaiacols ($R = 0.77$, Pearson) and syringols ($R = 0.83$, Pearson),
534 suggesting they were mainly derived from terrestrial higher plants. The decreasing trends of these
535 markers (relative abundance 10–40%) with increasing salinity, well aligned with $\delta^{13}\text{C}_{\text{org}}$ and BIT index,
536 further support the decreasing importance of terrestrial OM input towards the river mouth. In contrast,
537 N-compounds showed strong negative correlations with both guaiacols ($R = -0.84$, Pearson) and
538 syringols ($R = -0.81$, Pearson), suggesting a non-terrestrial OM origin such as protein from algal
539 detritus and chitin from various crustaceans (Nierop et al., 2017). *n*-Alkenes/alkanes, negatively
540 correlated with (terrestrial) polysaccharide-derived products ($R = -0.78$, Pearson; Fig. S2), were
541 probably from non-terrestrial sources like algaenan (de Leeuw et al., 2006). The other detected
542 pyrolysis products constituted a major fraction (> 50%) but most correlated with all mentioned source
543 proxies moderately or poorly ($-0.5 < R < 0.5$, Pearson; Fig. S2), thus are less effective provenance
544 proxies because they originate from multiple sources.

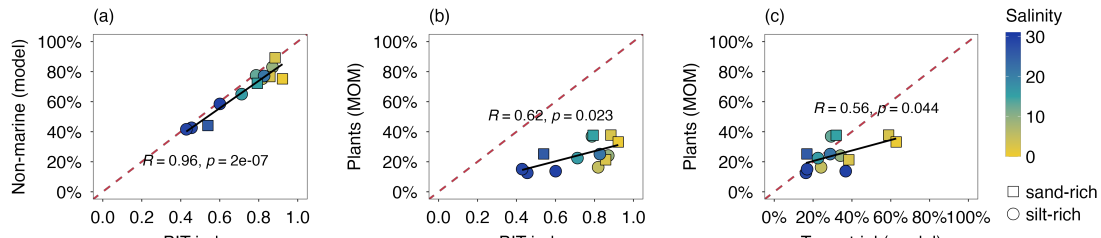
545

546 All proxies and analytical techniques have their strengths and weaknesses in determining OM
547 sources. Here, we obtain further insight into MOM characteristics by exploring the relationships
548 between different independent OM proxies and the end-member modelling results. There is a strong
549 agreement between the BIT index and the modelled non-marine OM contribution ($R = 0.96$, Pearson;
550 Fig. 8a), indicating that both approaches agree with respect to the relative contribution of terrestrial
551 sources (plants, rivers, soils) to the sedimentary OM pool. The contribution to the MOM pool by lignin-
552 derived products, likely representing remains of higher plants, was up to 40% (Fig. 8b) and correlated
553 strongly with BIT index ($R = 0.62$, Pearson). However, the weak slope in the scatter plot of BIT and
554 plant-MOM suggests that plant-derived OM was a lesser indicator of changes in OM composition and
555 reactivity in the harbor area. There was overall good agreement between the plant-derived
556 contribution from chemical MOM analysis and end-member modelling (Fig. 8c), indicating that mixing
557 models based on bulk OM parameters can provide valuable information about OM composition in
558 dynamic coastal settings.

559

560 The terrestrial OM fraction modelled from C/N and $\delta^{13}\text{C}_{\text{org}}$ showed a positive correlation with plant-
561 derived MOM pyrolysis products (Fig. 8c). Most data points seem to lie around the 1:1 curve except for
562 two sand-rich outliers. However, interpreting their relationship in Fig. 8c is challenging because of the
563 complexity in assigning MOM pyrolysis products to terrestrial-derived OM in estuarine environments.
564 Phenols and N-compounds, partially derived from terrestrial OM, are not included in the presented
565 MOM-determined contribution here. On the other hand, pyrolysis of algal material also produces
566 polysaccharide-derived products (Stevenson and Abbott, 2019), which can lead to overestimation of
567 MOM-determined terrestrial contribution. Nevertheless, this study suggests using bulk proxies (C/N,
568 $\delta^{13}\text{C}_{\text{org}}$) in combination with biomarker proxies (BIT index, MOM pyrolysis products) can provide a
569 more complete picture of OM composition in highly dynamic systems like estuaries.

570



571
572
573
574
575
576
577
578

Fig. 8. Scatter plots of proxies for OM source: (a) BIT index vs. non-marine OM contribution (i.e. terrestrial and riverine input from the three end-member modelling), (b) modelled terrestrial OM contribution vs. plant-derived MOM pyrolysis products (i.e. sum of guaiacols, syringols, polysaccharide-derived products), (c) BIT index vs. plant-derived MOM pyrolysis products (i.e. sum of guaiacols, syringols, polysaccharide-derived products). The red dashed lines are 1:1 curves and the black lines are the linear regression fitting curves.

579 **4.2 Organic matter degradation: rates and pathways**

580 In the 8-h whole-core incubation experiment, oxygen consumption was mostly due to OM
581 mineralization; the upward diffusive fluxes of reduced species (e.g. Fe^{2+} , HS^-) that can react with
582 oxygen represented a negligible oxygen sink at the sediment-water interface (< 1% of total oxygen
583 uptake; calculation detailed in the SI). The measured benthic O_2 consumption rates in the PoR
584 sediments ($33 \pm 6 \text{ mmol m}^{-2} \text{ d}^{-1}$) were similar to the reported rates in coastal sediments in the North
585 Sea ($22.1 \pm 0.6 \text{ mmol m}^{-2} \text{ d}^{-1}$; Neumann et al., 2021) and other human-influenced estuarine sediments
586 ($27\text{--}82 \text{ mmol m}^{-2} \text{ d}^{-1}$; Kraal et al., 2013). In estuarine systems, high primary production and shallow
587 water depth (here 13–25 m) lead to deposition of a substantial amount of freshly produced OM,
588 contributing to the high aerobic OM degradation rates. Furthermore, the whole-core incubation
589 showed similar O_2 consumption rates between sediment types. However, TOC-normalized carbon
590 emission rates from OM degradation—measured as DIC in the whole-core incubation and CO_2 in the
591 subaerial bottle incubation experiment—were higher in marine sediments compared to riverine
592 sediments (Fig. 5, 6). Here, the DIC_{OM} flux, which more broadly represents OM degradation in the
593 surface sediment as it includes anaerobic OM degradation pathways, was normalized to TOC in order
594 to compare between sites with strongly differing surface-sediment TOC contents (2.2 wt.% for site 115
595 vs. 5 wt.% for site 21A). The results indicate that short-term oxic respiration rates (Fig. 5a), driven by
596 rapid degradation of freshly deposited (algal) OM at the sediment-water interface, were similar
597 between sites. Furthermore, OM degradation rates may have been affected by (similar) limitation of
598 O_2 supply rather than carbon availability. By contrast, overall (Fig. 5d) and long-term (Fig. 6b) OM
599 degradation in the riverine sediment was 3–4 times slower than in the marine sediment, the former
600 being characterized by a higher proportion of more recalcitrant OM sources. This suggests a link
601 between OM composition and ‘quality’ (rather than quantity) and the CO_2 release potential from
602 (dredged) estuarine sediment. Sediment from site 115 likely received a greater supply and burial of
603 freshly produced (N-rich) algal OM, due to a faster burial rate ($10\text{--}15 \text{ cm yr}^{-1}$) than at riverine site 21A
604 ($<10 \text{ cm yr}^{-1}$; Cox et al., 2021). Riverine sediments (e.g. 21A), however, were richer in eroded soil OM
605 (Fig. 8), which is typically more recalcitrant and N-depleted than freshly produced algal OM.

606
607 Regarding the role of estuaries in carbon cycling, a crucial transition in anaerobic OM degradation
608 pathways is the onset of methanogenesis, which occurs when other TEAs have become depleted.
609 Due to a lower salinity and thus a shallowing of the sulfate-methane transition zone (Kuliński et al.,
610 2022), sediment from a river location (21A; salinity 5) exhibited an eight-time larger CH₄ efflux (Fig.
611 5c) compared to the marine location (115; salinity 29) despite of less degradable OM with a stronger
612 terrestrial signature (Fig. 2) as evidenced by the above-described lower OM mineralization rates
613 relative to TOC content. Similar spatial variability of benthic CH₄ fluxes as a function of salinity was
614 documented in other estuaries but with rather different values (0.2–19 mmol m⁻² d⁻¹; Gelesh et al.,
615 2016; Li et al., 2021; Middelburg et al., 2002). Note that the benthic fluxes measured here do not
616 directly translate into atmospheric CO₂ and CH₄ emissions, as various processes (e.g. carbonate
617 system equilibria, CH₄ oxidation) act on the speciation and concentration of these greenhouse gases
618 released from the sediment. Nevertheless, estuaries are considered as hotspots for both CO₂ and
619 CH₄ emissions into atmosphere (Li et al., 2023; Middelburg et al., 2002). Therefore, elucidating how in
620 addition to OM content the source and composition as well environmental conditions during OM
621 degradation control the magnitude and speciation of carbon release from estuarine sediment is
622 important to better constrain the role of estuaries in global carbon cycling.
623

624 **4.3 The impact of perturbation on organic matter degradation**

625 Sediment dredging and its further management, such as relocation on land, often alter OM
626 degradation conditions substantially by reintroducing O₂. In principle, aerobic degradation is more
627 effective than anaerobic degradation as aerobic oxidation has a relatively high energy yield, especially
628 compared to sulfate reduction (Hansen and Blackburn, 1991). This is reflected in the whole-core
629 incubation results, where aerobic mineralization confined in the uppermost few-millimeter-thick
630 sediment layer (Revsbech et al., 1980) accounted for 25–30% of the total OM-derived DIC production
631 across the entire 15-cm sediment core. By manually perturbing sediments and exposing them to
632 atmospheric oxygen in subaerial incubations, we found that the initial (day 2) TOC-normalized carbon
633 emission rate (283±42 and 134±29 µmol C g C⁻¹ d⁻¹ for 115 and 21A, respectively; Fig. 6b) increased
634 to 2–3 times of that in undisturbed whole-core incubation (158±61 and 41±12 µmol C g C⁻¹ d⁻¹ for 115
635 and 21A, respectively; Fig. 5d). These findings agree with a slurry incubation experiment under
636 contrasting redox conditions using Dutch coastal sediments conducted by (Dauwe et al., 2001), which
637 showed that the mineralization rate under aerobic conditions was faster than anaerobic conditions by
638 up to one order of magnitude. Furthermore, the increase in carbon emission rate was more
639 pronounced in the riverine sediment (21A) with a three-fold increase after perturbation, compared to
640 the marine sediment (115) with a two-fold increase. We attribute this to the stronger terrestrial,
641 recalcitrant signature of OM in the riverine part of the investigated harbor area. (Hulthe et al., 1998)
642 suggested that the impact of redox conditions and specifically oxygen availability is greatest for
643 relatively recalcitrant OM; fresh, labile OM is degraded relatively rapidly under aerobic and anaerobic
644 conditions. Therefore, the difference in the observed rate increase following sediment perturbation
645 may be attributed to the more active enzymatic catalysis involved in the degradation of terrestrial OM,

646 such as lignin, cellulose, and tannins (Hedges and Oades, 1997), compared to freshly produced
647 marine OM was more predominant.

648
649 These OM source-dependent differences in OM degradation rates were expressed across the six
650 investigated sites: the TOC-normalized carbon emission rates were over 100% higher in marine
651 sediments (115, 86, NWWG-02) than riverine sediments (21A, B16, K1v2) at almost all timesteps (Fig.
652 6b). This observed difference was supported by the OM end-member analysis: sediments near the
653 river mouth (115, 86, NWWG-02) were composed of more than 50% marine OM and less than 20%
654 terrestrial OM, whereas sediments from the river side (21A, B16, K1v2) were dominated (>70%) by
655 non-marine OM (Fig. 2c, Table S2). The faster degradation rate of marine OM, such as algae, which
656 was reported to be up to 10 times faster than terrestrial OM (Guillemette et al., 2013), likely explains
657 the higher TOC-normalized carbon emission rates in marine sediments. We note that sample
658 treatment for the subaerial bottle incubation experiment, i.e. freeze-drying and rewetting, may have
659 reduced overall microbial activities and thus OM degradability, but previous studies indicate that such
660 an effect is likely limited (He et al., 2022; Wu et al., 2020) and does not affect the overall conclusions
661 regarding the role of OM source and reactivity in shaping CO₂ emission kinetics.

662
663 In addition to the degradation rate, the extent of OM degradation is also affected by the OM source
664 and composition. By the end of the subaerial incubation experiment, marine sediments (115, 86,
665 NWWG-02) exhibited 2–4 times larger fractions of degraded TOC than riverine sediments (21A, B16,
666 K1v2; Fig. 7). Despite a lower TOC content, marine sediments contained a higher percentage of
667 fresher and more labile OM, thus resulting in a larger biodegradation fraction after 37 days of
668 subaerial incubation. A majority of the annual dredged sediment volume is marine (~77%; Kirichek et
669 al., 2018) and, consequently, dredging mostly perturbs sediments with relatively labile OM and high
670 potential CO₂ emission rates. Interestingly, sand-rich sediment NWWG-02 exhibited a notably larger
671 biodegradable OM fraction (up to 7%; Fig. 7), highlighting sediment texture may play an important role
672 besides OM sources. Silt-rich sediment can contain 20 times more mineral-associated OM than sand-
673 rich wetland soils (Mirabito and Chambers, 2023). This mineral-associated OM, physically protected
674 by inorganic matrices from mineralization, was suggested to play a key role in lasting carbon
675 sequestration globally (Georgiou et al., 2022; Keil et al., 1994).

676
677 Despite variations in the fractions of degraded TOC, more than 90% of the organic carbon remained
678 in the sediments by the end of the 37-day aerobic incubation experiments (Fig. 7). This aligns with
679 other studies where a majority fraction (> 80%) of organic carbon remained preserved in sediments or
680 soils after prolonged incubation periods ranging from weeks to years (Gebert et al., 2019; Haynes,
681 2005; Plante et al., 2011). The predominant fraction of sediment OM being less degradable on such
682 timescales fits well with the relatively large amounts (~50%) of pyrolysis products derived from
683 (terrestrial) polysaccharide, *n*-alkenes/alkanes from algaenan, guaiacols and syringols from lignin.
684 However, (Zander et al., 2022) indicated that the slow degradation of the majority of OM could also be
685 attributed to its association with sedimentary minerals. Importantly, the remaining OM, while resistant

686 to degradation over weeks to years, is still potentially degradable on longer timescales and relevant
687 for the carbon footprint of perturbing estuarine sediment over decades. While the results in this study
688 indicate that reintroduction of O₂ leads to a short-lived increase in estuarine OM degradation rates,
689 the degradation can still be stimulated under certain conditions. For instance, the addition of fresh,
690 readily degradable OM, known as priming, was reported to increase the degradability of old,
691 recalcitrant OM by 59% (Huo et al., 2017). This highlights that the organic carbon turnover rate is
692 rather complex and can vary markedly under different sediment management practices.

693

694 **4.4 Implications and future perspectives**

695 Estuaries are sites of high OM production and understanding OM processes within these regions is
696 key to quantify organic carbon budgets along the river-estuary-coastal ocean continuum (Canuel and
697 Hardison, 2016). In the PoR, sediment OM degradation (i.e. degradation rate and biodegradable pool)
698 exhibited a large spatial variation (marine vs. riverine), demonstrated in both whole-core and subaerial
699 incubation experiments. This spatial variability likely reflected a shift of OM composition, where marine
700 sediment was richer in freshly produced, easily degradable OM of algal origin. Similar source-
701 dependent OM degradation patterns were also observed in other coastal systems (e.g. the Elbe
702 estuary; Zander et al., 2022). However, the spatial distribution of OM may vary between different
703 estuaries, driven by many environmental factors (e.g. hydrological conditions, nutrient availability, land
704 use). Combining multiple independent proxies (e.g. C/N, $\delta^{13}\text{C}_{\text{org}}$, biomarkers) can improve our ability
705 to understand the source, transport and fate of OM in (perturbed) estuarine environments.
706 Degradation of OM is responsible for nutrient cycling, oxygen balance between the aquatic system
707 and sediment, and most early diagenetic processes (Middelburg et al., 1993). Therefore, recognizing
708 and differentiating OM reactivity of varying sources can help to refine the biogeochemical processes
709 and minimize the uncertainty in estimating OM mineralization and preservation efficiency in both field
710 and theoretical frameworks.

711

712 Anthropogenic perturbation like dredging within the coastal zone have greatly intensified in recent
713 decades. It is therefore important to explore the impact of such activities, specifically dredging and
714 potential sediment reuse, on the fate of carbon stored in estuarine sediments. The growing trend of
715 sediment reuse on land (e.g. beach nourishment, dike construction) introduces subaerial conditions
716 that can boost carbon mineralization rates (2–3 times), as shown in the open-air incubations. Current
717 practice with unpolluted PoR dredged sediment is relocation in the shallow North Sea, which is likely
718 to lead to less CO₂ emission than open-air incubation because (1) burial of dredged sediment at sea
719 limits exposure to O₂ and thus degradation rates and (2) buffering of released CO₂ in the water
720 column by conversion to HCO₃[−]. However, extensive resuspension in the coastal zone will increase
721 O₂ exposure and CO₂ release into seawater results in a pH decrease, and as such the reactivity of
722 dredged material as determined in this study is also relevant to inform about the environmental impact
723 of disposal at sea. Overall, balancing sediment valorization with its associated carbon footprint is of
724 importance in determining the suitable sediment management strategies.

725

726 Methane, a strong greenhouse gas, is often oversaturated in the OM-rich coastal sediments, favoring
727 CH₄ bubble formation. Most CH₄ is trapped below the sulfate-methane transition zone, within which
728 anaerobic oxidation of methane (AOM) coupled to SO₄²⁻ removes approximately 71% of the CH₄ in
729 marine sediments (Gao et al., 2022). Dredging, similar to the natural forms of sediment erosion (Hulot
730 et al., 2023), can disrupt the functioning of this AOM filter and destabilize riverbed/seabed, leading to
731 a temporary CH₄ escape via enhanced diffusion and ebullition (Maeck et al., 2013; Nijman et al.,
732 2022). However, in the long term, exposing sediments to oxygen is expected to inhibit methane
733 production and emissions (Nijman et al., 2022). Whether dredging and the following sediment
734 processing will shift the estuarine sediment from a carbon sink into a carbon source is dependent on
735 the pristine sediment carbon dynamics and the specifications of human disturbance. Indubitably,
736 estuaries will remain vulnerable to human pressure and climate change. These alternations will in
737 return influence the important drivers of the estuarine, further affecting the balance between OM
738 degradation and preservation (Heckbert et al., 2012).

739

740 **Conclusions**

741 The PoR sediments, like many other coastal sediments, exhibited relatively high OM content and
742 reactivity due to the high primary production and rapid sedimentation in these shallow aquatic
743 systems. Organic carbon in marine sediments degraded up to 5 times faster than that in riverine
744 sediments under both intact and perturbed conditions. This variability was suggested to reflect
745 differences in OM composition: marine sediments were richer in recently produced, labile algal OM.
746 By contrast, riverine sediments contained larger amounts of eroded, more recalcitrant soil and plant-
747 derived OM. Additionally, OM degradation rates were 2–3 times higher in the open-air, disturbed
748 sediment incubations than the intact whole-core incubations. This suggested that perturbation
749 triggered by sediment dredging and processing can mobilize the sequestered sediment organic
750 carbon. Despite only 1–7% of organic carbon was released after 37-day open-air incubation, certain
751 favorable conditions may still promote degradation of the remaining organic carbon. With the growing
752 need for dredging and other coastal sediment reworking, it is therefore of great importance to
753 consider the sensitivity of carbon in sediment management practices on relevant timescales and in
754 the context of the fast-changing environmental conditions.

755

756

757

758

759 **Author contribution**

760 GW conceptualized the study, developed the methodology, conducted the investigation and formal
761 analysis, created visualizations, and wrote the original draft of the manuscript. KN and BY contributed
762 to the investigation and formal analysis, and reviewed and edited the manuscript. SS and GJR
763 reviewed and edited the manuscript. PK supervised the project, contributed to the conceptualization
764 and methodology, acquired funding, and reviewed and edited the manuscript. All authors reviewed
765 and agreed on the final version of the manuscript.

766

767 **Data availability**

768 The datasets used in this study are available from the corresponding author upon reasonable request.

769

770 **Declaration of competing interest**

771 The authors declare no competing interests.

772

773 **Acknowledgements**

774 This study is part of the project 'Transforming harbor sediment from waste into resource' funded by
775 the Exact and Natural Sciences domain of the Dutch Research Council, NWO (grant number
776 TWM.BL.019.005). We extend our gratitude to the Port of Rotterdam Authority, particularly Marco
777 Wensveen and Ronald Rutgers, and Heijdra Milieu Service B.V. for their assistance with sediment
778 collection. We thank Julia Gebert from Delft University of Technology for her stimulating discussion.
779 We appreciate the scientific and technical staff from NIOZ Royal Netherlands Institute for Sea
780 Research for their analytical support.

781

782 **Appendix A. Supplementary data**

783 The online version contains supplementary material available at XXX.

784

785

786

787 **References**

788 Aller, R. C.: Bioturbation and remineralization of sedimentary organic matter: effects of redox
789 oscillation, *Chem Geol*, 114, 331–345, [https://doi.org/10.1016/0009-2541\(94\)90062-0](https://doi.org/10.1016/0009-2541(94)90062-0), 1994.

790 Amar, M., Benzerzour, M., Kleib, J., and Abriak, N. E.: From dredged sediment to supplementary
791 cementitious material: characterization, treatment, and reuse, *International Journal of Sediment
792 Research*, 36, 92–109, <https://doi.org/10.1016/j.ijsrc.2020.06.002>, 2021.

793 Arndt, S., Jørgensen, B. B., LaRowe, D. E., Middelburg, J. J., Pancost, R. D., and Regnier, P.:
794 Quantifying the degradation of organic matter in marine sediments: A review and synthesis, *Earth Sci
795 Rev*, 123, 53–86, <https://doi.org/10.1016/j.earscirev.2013.02.008>, 2013.

796 Barbier, E. B., Hacker, S. D., Kennedy, C., Koch, E. W., Stier, A. C., and Silliman, B. R.: The value of
797 estuarine and coastal ecosystem services, *Ecol Monogr*, 81, 169–193, <https://doi.org/10.1890/10-1510.1>, 2011.

799 Bauer, J. E., Cai, W. J., Raymond, P. A., Bianchi, T. S., Hopkinson, C. S., and Regnier, P. A. G.: The
800 changing carbon cycle of the coastal ocean, *Nature*, 504, 61–70, <https://doi.org/10.1038/nature12857>,
801 2013.

802 Bianchi, T. S. and Bauer, J. E.: Particulate Organic Carbon Cycling and Transformation, Elsevier Inc.,
803 69–117 pp., <https://doi.org/10.1016/B978-0-12-374711-2.00503-9>, 2012.

804 Bianchi, T. S., Cui, X., Blair, N. E., Burdige, D. J., Eglinton, T. I., and Galy, V.: Centers of organic
805 carbon burial and oxidation at the land-ocean interface, *Org Geochem*, 115, 138–155,
806 <https://doi.org/10.1016/j.orggeochem.2017.09.008>, 2018.

807 Brandini, N., da Costa Machado, E., Sanders, C. J., Cotovicz, L. C., Bernardes, M. C., and Knoppers,
808 B. A.: Organic matter processing through an estuarine system: Evidence from stable isotopes ($\delta^{13}\text{C}$
809 and $\delta^{15}\text{N}$) and molecular (lignin phenols) signatures, *Estuar Coast Shelf Sci*, 265,
810 <https://doi.org/10.1016/j.ecss.2021.107707>, 2022.

811 Burd, A. B., Frey, S., Cabre, A., Ito, T., Levine, N. M., Lønborg, C., Long, M., Mauritz, M., Thomas, R.
812 Q., Stephens, B. M., Vanwalleghem, T., and Zeng, N.: Terrestrial and marine perspectives on
813 modeling organic matter degradation pathways, *Glob Chang Biol*, 22, 121–136,
814 <https://doi.org/10.1111/gcb.12987>, 2016.

815 Burdige, D. J.: Preservation of organic matter in marine sediments: Controls, mechanisms, and an
816 imbalance in sediment organic carbon budgets?, *Chem Rev*, 107, 467–485,
817 <https://doi.org/10.1021/cr050347q>, 2007.

818 Burdige, D. J.: Estuarine and Coastal Sediments - Coupled Biogeochemical Cycling, Elsevier Inc.,
819 279–316 pp., <https://doi.org/10.1016/B978-0-12-374711-2.00511-8>, 2012.

820 Buurman, P., Nierop, K. G. J., Pontevedra-Pombal, X., and Martínez Cortizas, A.: Chapter 10
821 Molecular chemistry by pyrolysis-GC/MS of selected samples of the Penido Vello peat deposit,
822 Galicia, NW Spain, *Developments in Earth Surface Processes*, 9, 217–240,
823 [https://doi.org/10.1016/S0928-2025\(06\)09010-9](https://doi.org/10.1016/S0928-2025(06)09010-9), 2006.

824 Canuel, E. A. and Hardison, A. K.: Sources, Ages, and Alteration of Organic Matter in Estuaries, *Ann
825 Rev Mar Sci*, 8, 409–434, <https://doi.org/10.1146/annurev-marine-122414-034058>, 2016.

826 Cao, C., Cai, F., Qi, H., Zhao, S., and Wu, C.: Differences in the sulfate–methane transitional zone in
827 coastal pockmarks in various sedimentary environments, *Water (Switzerland)*, 13, 1–18,
828 <https://doi.org/10.3390/w13010068>, 2021.

829 Carneiro, L. M., do Rosário Zucchi, M., de Jesus, T. B., da Silva Júnior, J. B., and Hadlich, G. M.:
830 $\delta^{13}\text{C}$, $\delta^{15}\text{N}$ and TOC/TN as indicators of the origin of organic matter in sediment samples from the
831 estuary of a tropical river, *Mar Pollut Bull*, 172, <https://doi.org/10.1016/j.marpolbul.2021.112857>, 2021.

832 Chow, W. L., Chong, S., Lim, J. W., Chan, Y. J., Chong, M. F., Tiong, T. J., Chin, J. K., Pan, G. T.,
833 Puyuelo, B., Ponsá, S., Gea, T., Sánchez, A., Szulc, W., Rutkowska, B., Gawroński, S., and
834 Wszelaczyńska, E.: Determining C/N ratios for typical organic wastes using biodegradable fractions,
835 *Processes*, 85, 653–659, <https://doi.org/10.3390/pr9091501>, 2020.

836 Cloern, J. E., Canuel, E. A., and Harris, D.: Stable carbon and nitrogen isotope composition of aquatic
837 and terrestrial plants of the San Francisco Bay estuarine system, *Limnol Oceanogr*, 47, 713–729,
838 <https://doi.org/10.4319/lo.2002.47.3.0713>, 2002.

839 Cox, J. R., Dunn, F. E., Nienhuis, J. H., van der Perk, M., and Kleinhans, M. G.: Climate change and
840 human influences on sediment fluxes and the sediment budget of an urban delta: The example of the

841 lower rhine-meuse delta distributary network, *Anthropocene Coasts*, 4, 251–280,
842 <https://doi.org/10.1139/anc-2021-0003>, 2021.

843 Dauwe, B., Middelburg, J. J., and Herman, P. M. J.: Effect of oxygen on the degradability of organic
844 matter in subtidal and intertidal sediments of the North Sea area, 215, 13–22, 2001.

845 Dür, H. H., Laruelle, G. G., van Kempen, C. M., Slomp, C. P., Meybeck, M., and Middelkoop, H.:
846 Worldwide Typology of Nearshore Coastal Systems: Defining the Estuarine Filter of River Inputs to
847 the Oceans, *Estuaries and Coasts*, 34, 441–458, <https://doi.org/10.1007/s12237-011-9381-y>, 2011.

848 Egger, M., Riedinger, N., Mogollón, J. M., and Jørgensen, B. B.: Global diffusive fluxes of methane in
849 marine sediments, *Nat Geosci*, 11, 421–425, <https://doi.org/10.1038/s41561-018-0122-8>, 2018.

850 Fabbri, D., Sangiorgi, F., and Vassura, I.: Pyrolysis-GC-MS to trace terrigenous organic matter in
851 marine sediments: A comparison between pyrolytic and lipid markers in the Adriatic Sea, *Anal Chim
852 Acta*, 530, 253–261, <https://doi.org/10.1016/j.aca.2004.09.020>, 2005.

853 Fairbairn, L., Rezanezhad, F., Gharasoo, M., Parsons, C. T., Macrae, M. L., Slowinski, S., and Van
854 Cappellen, P.: Relationship between soil CO₂ fluxes and soil moisture: Anaerobic sources explain
855 fluxes at high water content, *Geoderma*, 434, 116493,
856 <https://doi.org/10.1016/j.geoderma.2023.116493>, 2023.

857 Finlay, J. C. and Kendall, C.: Stable Isotope Tracing of Temporal and Spatial Variability in Organic
858 Matter Sources to Freshwater Ecosystems, in: *Stable Isotopes in Ecology and Environmental
859 Science*, edited by: Michener, R. and Lajtha, Wiley, 283–333,
860 <https://doi.org/10.1002/9780470691854.ch10>, 2007.

861 Freitas, F. S., Pika, P. A., Kasten, S., Jorgensen, B. B., Rassmann, J., Rabouille, C., Thomas, S.,
862 Sass, H., Pancost, R. D., and Arndt, S.: New insights into large-scale trends of apparent organic
863 matter reactivity in marine sediments and patterns of benthic carbon transformation, *Biogeosciences*,
864 18, 4651–4679, <https://doi.org/10.5194/bg-18-4651-2021>, 2021.

865 Gao, Y., Wang, Y., Lee, H. S., and Jin, P.: Significance of anaerobic oxidation of methane (AOM) in
866 mitigating methane emission from major natural and anthropogenic sources: a review of AOM rates in
867 recent publications, *Environmental Science: Advances*, 1, 401–425,
868 <https://doi.org/10.1039/d2va00091a>, 2022.

869 Gebert, J., Knoblauch, C., and Gröngröft, A.: Gas production from dredged sediment, *Waste
870 Management*, 85, 82–89, <https://doi.org/10.1016/j.wasman.2018.12.009>, 2019.

871 Gelesh, L., Marshall, K., Boicourt, W., and Lapham, L.: Methane concentrations increase in bottom
872 waters during summertime anoxia in the highly eutrophic estuary, Chesapeake Bay, U.S.A., *Limnol
873 Oceanogr*, 61, S253–S266, <https://doi.org/10.1002/lno.10272>, 2016.

874 Georgiou, K., Jackson, R. B., Vinušková, O., Abramoff, R. Z., Ahlström, A., Feng, W., Harden, J. W.,
875 Pellegrini, A. F. A., Polley, H. W., Soong, J. L., Riley, W. J., and Torn, M. S.: Global stocks and
876 capacity of mineral-associated soil organic carbon, *Nat Commun*, 13, 1–12,
877 <https://doi.org/10.1038/s41467-022-31540-9>, 2022.

878 Guillemette, F., McCallister, S. L., and Del Giorgio, P. A.: Differentiating the degradation dynamics of
879 algal and terrestrial carbon within complex natural dissolved organic carbon in temperate lakes, *J
880 Geophys Res Biogeosci*, 118, 963–973, <https://doi.org/10.1002/jgrg.20077>, 2013.

881 Hansen, L. S. and Blackburn, T. H.: Aerobic and anaerobic mineralization of organic material in
882 marine sediment microcosms, *Mar Ecol Prog Ser*, 75, 283–291, <https://doi.org/10.3354/meps075283>,
883 1991.

884 Haynes, R. J.: Labile Organic Matter Fractions as Central Components of the Quality of Agricultural
885 Soils: An Overview, *Advances in Agronomy*, 85, 221–268, [https://doi.org/10.1016/S0065-2113\(04\)85005-3](https://doi.org/10.1016/S0065-
886 2113(04)85005-3), 2005.

887 He, Y., Zhang, T., Zhao, Q., Gao, X., He, T., and Yang, S.: Response of GHG emissions to interactions
888 of temperature and drying in the karst wetland of the Yunnan-Guizhou Plateau, *Front Environ Sci*, 10,
889 <https://doi.org/10.3389/fenvs.2022.973900>, 2022.

890 Heckbert, S., Costanza, R., Poloczanska, E. S., and Richardson, A. J.: Climate Regulation as a
891 Service from Estuarine and Coastal Ecosystems, Elsevier Inc., 199–216 pp.,
892 <https://doi.org/10.1016/B978-0-12-374711-2.01211-0>, 2012.

893 Hedges, J. I. and Oades, J. M.: Comparative organic geochemistries of soils and marine sediments,
894 *Org Geochem*, 27, 319–361, [https://doi.org/10.1016/S0146-6380\(97\)00056-9](https://doi.org/10.1016/S0146-6380(97)00056-9), 1997.

895 Herfort, L., Schouten, S., Boon, J. P., Woltering, M., Baas, M., Weijers, J. W. H., and Sinninghe
896 Damsté, J. S.: Characterization of transport and deposition of terrestrial organic matter in the southern
897 North Sea using the BIT index, *Limnol Oceanogr*, 51, 2196–2205,
898 <https://doi.org/10.4319/lo.2006.51.5.2196>, 2006.

899 Holligan, P. M. and Reiners, W. A.: Predicting the Responses of the Coastal Zone to Global Change,
900 *Adv Ecol Res*, 22, 211–255, [https://doi.org/10.1016/S0065-2504\(08\)60137-3](https://doi.org/10.1016/S0065-2504(08)60137-3), 1992.

901 Hopmans, E. C., Weijers, J. W. H., Schefuß, E., Herfort, L., Sinninghe Damsté, J. S., and Schouten,
902 S.: A novel proxy for terrestrial organic matter in sediments based on branched and isoprenoid
903 tetraether lipids, *Earth Planet Sci Lett*, 224, 107–116, <https://doi.org/10.1016/j.epsl.2004.05.012>, 2004.

904 Hopmans, E. C., Schouten, S., and Sinninghe Damsté, J. S.: The effect of improved chromatography
905 on GDGT-based palaeoproxies, *Org Geochem*, 93, 1–6,
906 <https://doi.org/10.1016/j.orggeochem.2015.12.006>, 2016.

907 Hulot, V., Metzger, E., Thibault de Chanvalon, A., Mouret, A., Schmidt, S., Deflandre, B., Rigaud, S.,
908 Beneteau, E., Savoye, N., Souchu, P., Le Merrer, Y., and Maillet, G. M.: Impact of an exceptional
909 winter flood on benthic oxygen and nutrient fluxes in a temperate macrotidal estuary: Potential
910 consequences on summer deoxygenation, *Front Mar Sci*, 10,
911 <https://doi.org/10.3389/fmars.2023.1083377>, 2023.

912 Hulthe, G., Hulth, S., and Hall, P. O. J.: Effect of oxygen on degradation rate of refractory and labile
913 organic matter in continental margin sediments, *Geochim Cosmochim Acta*, 62, 1319–1328,
914 [https://doi.org/10.1016/S0016-7037\(98\)00044-1](https://doi.org/10.1016/S0016-7037(98)00044-1), 1998.

915 Huo, C., Luo, Y., and Cheng, W.: Rhizosphere priming effect: A meta-analysis, *Soil Biol Biochem*, 111,
916 78–84, <https://doi.org/10.1016/j.soilbio.2017.04.003>, 2017.

917 Hutchings, J. A., Bianchi, T. S., Najjar, R. G., Herrmann, M., Kemp, W. M., Hinson, A. L., and Feagin,
918 R. A.: Carbon Deposition and Burial in Estuarine Sediments of the Contiguous United States, *Global
919 Biogeochem Cycles*, 34, <https://doi.org/10.1029/2019GB006376>, 2020.

920 IJsseldijk, L. L., Camphuysen, K. C. J., Nauw, J. J., and Aarts, G.: Going with the flow: Tidal influence
921 on the occurrence of the harbour porpoise (*Phocoena phocoena*) in the Marsdiep area, The
922 Netherlands, *J Sea Res*, 103, 129–137, <https://doi.org/10.1016/j.seares.2015.07.010>, 2015.

923 Jørgensen, B. B., Wenzhöfer, F., Egger, M., and Glud, R. N.: Sediment oxygen consumption: Role in
924 the global marine carbon cycle, *Earth Sci Rev*, 228, <https://doi.org/10.1016/j.earscirev.2022.103987>,
925 2022.

926 Kaal, J.: Analytical pyrolysis in marine environments revisited, *Analytical Pyrolysis Letters*, 1–16,
927 2019.

928 Kaal, J., Martínez Cortizas, A., Mateo, M. Á., and Serrano, O.: Deciphering organic matter sources
929 and ecological shifts in blue carbon ecosystems based on molecular fingerprinting, *Science of the
930 Total Environment*, 742, 140554, <https://doi.org/10.1016/j.scitotenv.2020.140554>, 2020.

931 Keil, R., Montluçon, D., Prahl, F., and Hedges, J.: Sorptive preservation of labile organic matter in
932 marine sediments, *Nature*, 370, 549–552, <https://doi.org/https://doi.org/10.1038/370549a0>, 1994.

933 Kirichek, A., Rutgers, R., Wenssween, M., and van Hassent, A.: Sediment management in the Port of
934 Rotterdam, in: *Baggern - Unterbringen - Aufbereiten - Verwerten*, Steinbeis-Transverzentrum
935 Angewandte Landschaftsplanung, 1–8, 2018.

936 Kraal, P., Burton, E. D., Rose, A. L., Cheetham, M. D., Bush, R. T., and Sullivan, L. A.: Decoupling
937 between water column oxygenation and benthic phosphate dynamics in a shallow eutrophic estuary,
938 *Environ Sci Technol*, 47, 3114–3121, <https://doi.org/10.1021/es304868t>, 2013.

939 Kuliński, K., Rehder, G., Asmala, E., Bartosova, A., Carstensen, J., Gustafsson, B., Hall, P. O. J.,
940 Humborg, C., Jilbert, T., Jürgens, K., Meier, H. E. M., Müller-Karulis, B., Naumann, M., Olesen, J. E.,
941 Savchuk, O., Schramm, A., Slomp, C. P., Sofiev, M., Sobek, A., Szymczycha, B., and Undeman, E.:
942 Biogeochemical functioning of the Baltic Sea, <https://doi.org/10.5194/esd-13-633-2022>, 2022.

943 Kuwae, T., Kanda, J., Kubo, A., Nakajima, F., Ogawa, H., Sohma, A., and Suzumura, M.: Blue carbon
944 in human-dominated estuarine and shallow coastal systems, *Ambio*, 45, 290–301,
945 <https://doi.org/10.1007/s13280-015-0725-x>, 2016.

946 Lamb, A. L., Wilson, G. P., and Leng, M. J.: A review of coastal palaeoclimate and relative sea-level
947 reconstructions using $\delta^{13}\text{C}$ and C/N ratios in organic material, *Earth Sci Rev*, 75, 29–57,
948 <https://doi.org/10.1016/j.earscirev.2005.10.003>, 2006.

950 LaRowe, D. E. and Van Cappellen, P.: Degradation of natural organic matter: A thermodynamic
951 analysis, *Geochim Cosmochim Acta*, 75, 2030–2042, <https://doi.org/10.1016/j.gca.2011.01.020>, 2011.

952 LaRowe, D. E., Arndt, S., Bradley, J. A., Estes, E. R., Hoar frost, A., Lang, S. Q., Lloyd, K. G.,
953 Mahmoudi, N., Orsi, W. D., Shah Walter, S. R., Steen, A. D., and Zhao, R.: The fate of organic carbon
954 in marine sediments - New insights from recent data and analysis, *Earth Sci Rev*, 204, 103146,
955 <https://doi.org/10.1016/j.earscirev.2020.103146>, 2020.

956 Laruelle, G. G., Dürr, H. H., Slomp, C. P., and Borges, A. V.: Evaluation of sinks and sources of CO₂
957 in the global coastal ocean using a spatially-explicit typology of estuaries and continental shelves,
958 *Geophys Res Lett*, 37, 1–6, <https://doi.org/10.1029/2010GL043691>, 2010.

959 de Leeuw, J. W., Versteegh, G. J. M., and van Bergen, P. F.: Biomacromolecules of algae and plants
960 and their fossil analogues, *Plant Ecol*, 182, 209–233, <https://doi.org/10.1007/s11258-005-9027-x>,
961 2006.

962 Li, M., Guo, Y., Cai, W. J., Testa, J. M., Shen, C., Li, R., and Su, J.: Projected increase in carbon
963 dioxide drawdown and acidification in large estuaries under climate change, *Commun Earth Environ*,
964 4, 1–10, <https://doi.org/10.1038/s43247-023-00733-5>, 2023.

965 Li, Y., Zhan, L., Chen, L., Zhang, J., Wu, M., and Liu, J.: Spatial and temporal patterns of methane
966 and its influencing factors in the Jiulong River estuary, southeastern China, *Mar Chem*, 228, 103909,
967 <https://doi.org/10.1016/j.marchem.2020.103909>, 2021.

968 Lovley, D. R. and Phillips, E. J. P.: Availability of Ferric Iron for Microbial Reduction in Bottom
969 Sediments of the Freshwater Tidal Potomac River, *Appl Environ Microbiol*, 52,
970 <https://doi.org/https://doi.org/10.1128/aem.52.4.751-757.1986>, 1986.

971 Macreadie, P. I., Anton, A., Raven, J. A., Beaumont, N., Connolly, R. M., Friess, D. A., Kelleway, J. J.,
972 Kennedy, H., Kuwae, T., Lavery, P. S., Lovelock, C. E., Smale, D. A., Apostolaki, E. T., Atwood, T. B.,
973 Baldock, J., Bianchi, T. S., Chmura, G. L., Eyre, B. D., Fourqurean, J. W., Hall-Spencer, J. M.,
974 Huxham, M., Hendriks, I. E., Krause-Jensen, D., Laffoley, D., Luisetti, T., Marbà, N., Masque, P.,
975 McGlathery, K. J., Megonigal, J. P., Murdiyarso, D., Russell, B. D., Santos, R., Serrano, O., Silliman,
976 B. R., Watanabe, K., and Duarte, C. M.: The future of Blue Carbon science, *Nat Commun*, 10, 1–13,
977 <https://doi.org/10.1038/s41467-019-11693-w>, 2019.

978 Maeck, A., Delsontro, T., McGinnis, D. F., Fischer, H., Flury, S., Schmidt, M., Fietzek, P., and Lorke, A.:
979 Sediment trapping by dams creates methane emission hot spots, *United States of America,*
980 *Environmental Science and Technology*, 8130–8137, 2013.

981 Magen, C., Lapham, L. L., Pohlman, J. W., Marshall, K., Bosman, S., Casso, M., and Chanton, J. P.: A
982 simple headspace equilibration method for measuring dissolved methane, *Limnol Oceanogr Methods*,
983 12, 637–650, <https://doi.org/10.4319/lom.2014.12.637>, 2014.

984 McLeod, E., Chmura, G. L., Bouillon, S., Salm, R., Björk, M., Duarte, C. M., Lovelock, C. E.,
985 Schlesinger, W. H., and Silliman, B. R.: A blueprint for blue carbon: Toward an improved
986 understanding of the role of vegetated coastal habitats in sequestering CO₂, *Front Ecol Environ*, 9,
987 552–560, <https://doi.org/10.1890/110004>, 2011.

988 Middelburg, J. J. and Herman, P. M. J.: Organic matter processing in tidal estuaries, *Mar Chem*, 106,
989 127–147, <https://doi.org/10.1016/j.marchem.2006.02.007>, 2007.

990 Middelburg, J. J. and Nieuwenhuize, J.: Carbon and nitrogen stable isotopes in suspended matter and
991 sediments from the Schelde Estuary, *Mar Chem*, 60, 217–225, [https://doi.org/10.1016/S0304-4203\(97\)00104-7](https://doi.org/10.1016/S0304-4203(97)00104-7), 1998.

993 Middelburg, J. J., Vlug, T., Jaco, F., and van der Nat, W. A.: Organic matter mineralization in marine
994 systems, *Glob Planet Change*, 8, 47–58, [https://doi.org/10.1016/0921-8181\(93\)90062-S](https://doi.org/10.1016/0921-8181(93)90062-S), 1993.

995 Middelburg, J. J., Nieuwenhuize, J., Iversen, N., Høgh, N., De Wilde, H., Helder, W., Seifert, R., and
996 Christof, O.: Methane distribution in European tidal estuaries, *Biogeochemistry*, 59, 95–119,
997 <https://doi.org/10.1023/A:1015515130419>, 2002.

998 Mirabito, A. J. and Chambers, L. G.: Quantifying mineral-associated organic matter in wetlands as an
999 indicator of the degree of soil carbon protection, *Geoderma*, 430, 116327,
1000 <https://doi.org/10.1016/j.geoderma.2023.116327>, 2023.

1001 Neumann, A., van Beusekom, J. E. E., Eisele, A., Emeis, K. C., Friedrich, J., Kröncke, I., Logemann,
1002 E. L., Meyer, J., Naderipour, C., Schückel, U., Wrede, A., and Zettler, M. L.: Macrofauna as a major
1003 driver of benthic-pelagic exchange in the southern North Sea, *Limnol Oceanogr*, 66, 2203–2217,
1004 <https://doi.org/10.1002/lno.11748>, 2021.

1005 Nierop, K. G. J., Reichart, G. J., Veld, H., and Sinninghe Damsté, J. S.: The influence of oxygen
1006 exposure time on the composition of macromolecular organic matter as revealed by surface
1007 sediments on the Murray Ridge (Arabian Sea), *Geochim Cosmochim Acta*, 206, 40–56,
1008 <https://doi.org/10.1016/j.gca.2017.02.032>, 2017.

1009 Nijman, T. P. A., Lemmens, M., Lurding, M., Kosten, S., Welte, C., and Veraart, A. J.: Phosphorus
1010 control and dredging decrease methane emissions from shallow lakes, *Science of the Total
1011 Environment*, 847, 157584, <https://doi.org/10.1016/j.scitotenv.2022.157584>, 2022.

1012 Plante, A. F., Fernández, J. M., Haddix, M. L., Steinweg, J. M., and Conant, R. T.: Biological, chemical
1013 and thermal indices of soil organic matter stability in four grassland soils, *Soil Biol Biochem*, 43,
1014 1051–1058, <https://doi.org/10.1016/j.soilbio.2011.01.024>, 2011.

1015 Puyuelo, B., Ponsá, S., Gea, T., and Sánchez, A.: Determining C/N ratios for typical organic wastes
1016 using biodegradable fractions, *Chemosphere*, 85, 653–659,
1017 <https://doi.org/10.1016/j.chemosphere.2011.07.014>, 2011.

1018 Revsbech, N. P., Sorensen, J., Blackburn, T. H., and Lomholt, J. P.: Distribution of oxygen in marine
1019 sediments measured with microelectrodes, *Limnol Oceanogr*, 25, 403–411,
1020 <https://doi.org/10.4319/lo.1980.25.3.0403>, 1980.

1021 Schouten, S., Hopmans, E. C., and Sinninghe Damsté, J. S.: The organic geochemistry of glycerol
1022 dialkyl glycerol tetraether lipids: A review, *Org Geochem*, 54, 19–61,
1023 <https://doi.org/10.1016/j.orggeochem.2012.09.006>, 2013.

1024 Schulz, H. and Zabel, M.: *Marine Geochemistry*, Springer Berlin Heidelberg New York, 132 pp., 2006.

1025 Shao, L., Wu, D., Zhang, D., and Feng, T.: Using Isotopes to Identify the Sources of Organic Carbon
1026 and Nitrogen in Surface Sediment in Shallow Lakes Alongside Poyang Lake, *Wetlands*, 39, 25–33,
1027 <https://doi.org/10.1007/s13157-017-0988-z>, 2019.

1028 Smith, R. W., Bianchi, T. S., and Savage, C.: Comparison of lignin phenols and branched/isoprenoid
1029 tetraethers (BIT index) as indices of terrestrial organic matter in Doubtful Sound, Fiordland, New
1030 Zealand, *Org Geochem*, 41, 281–290, <https://doi.org/10.1016/j.orggeochem.2009.10.009>, 2010.

1031 Steele, J. H., Thorpe, S. A., and Turekian, K. K.: *Marine Chemistry & Geochemistry*, edited by: Steele,
1032 J. H., Thorpe, S. A., and Turekian, K. K., 2010.

1033 Stevenson, M. A. and Abbott, G. D.: Exploring the composition of macromolecular organic matter in
1034 Arctic Ocean sediments under a changing sea ice gradient, *J Anal Appl Pyrolysis*, 140, 102–111,
1035 <https://doi.org/10.1016/j.jaat.2019.02.006>, 2019.

1036 Stock, B. C., Jackson, A. L., Ward, E. J., Parnell, A. C., Phillips, D. L., and Semmens, B. X.: Analyzing
1037 mixing systems using a new generation of Bayesian tracer mixing models, *PeerJ*, 2018, 1–27,
1038 <https://doi.org/10.7717/peerj.5096>, 2018.

1039 Strong, D. J., Flecker, R., Valdes, P. J., Wilkinson, I. P., Rees, J. G., Zong, Y. Q., Lloyd, J. M., Garrett,
1040 E., and Pancost, R. D.: Organic matter distribution in the modern sediments of the Pearl River
1041 Estuary, *Org Geochem*, 49, 68–82, <https://doi.org/10.1016/j.orggeochem.2012.04.011>, 2012.

1042 Stronkhorst, J. and Van Hattum, B.: Contaminants of concern in Dutch marine harbor sediments, *Arch
1043 Environ Contam Toxicol*, 45, 306–316, <https://doi.org/10.1007/s00244-003-0191-5>, 2003.

1044 Szulc, W., Rutkowska, B., Gawroński, S., and Wszelaczyńska, E.: Possibilities of using organic waste
1045 after biological and physical processing—an overview, *Processes*, 9,
1046 <https://doi.org/10.3390/pr9091501>, 2021.

1047 Thornton, S. F. and McManus, J.: Application of organic carbon and nitrogen stable isotope and C/N
1048 ratios as source indicators of organic matter provenance in estuarine systems: Evidence from the Tay
1049 estuary, Scotland, *Estuar Coast Shelf Sci*, 38, 219–233, <https://doi.org/10.1006/ecss.1994.1015>,
1050 1994.

1051 Tumuluru, J. S., Hess, J. R., Boardman, R. D., Wright, C. T., and Westover, T. L.: Formulation,
1052 pretreatment, and densification options to improve biomass specifications for Co-firing high
1053 percentages with coal, *Industrial Biotechnology*, 8, 113–132, <https://doi.org/10.1089/ind.2012.0004>,
1054 2012.

1055 van de Velde, S., van Lancker, V., Hidalgo-Martinez, S., Berelson, W. M., and Meysman, F. J. R.:
1056 Anthropogenic disturbance keeps the coastal seafloor biogeochemistry in a transient state, *Sci Rep*,
1057 8, 1–10, <https://doi.org/10.1038/s41598-018-23925-y>, 2018.

1058 Wakeham, S. G. and Canuel, E. A.: Degradation and preservation of organic matter in marine
1059 sediments, *Handbook of Environmental Chemistry*, Volume 2: Reactions and Processes, 2 N, 295–
1060 321, https://doi.org/10.1007/698_2_009, 2006.

1061 Wiesner, M. G., Haake, B., and Wirth, H.: Organic facies of surface sediments in the North Sea, *Org*
1062 *Geochem*, 15, 419–432, [https://doi.org/10.1016/0146-6380\(90\)90169-Z](https://doi.org/10.1016/0146-6380(90)90169-Z), 1990.

1063 Wu, D., Deng, L., Liu, Y., Xi, D., Zou, H., Wang, R., Sha, Z., Pan, Y., Hou, L., and Liu, M.:
1064 Comparisons of the effects of different drying methods on soil nitrogen fractions: Insights into
1065 emissions of reactive nitrogen gases (HONO and NO), *Atmospheric and Oceanic Science Letters*, 13,
1066 224–231, <https://doi.org/10.1080/16742834.2020.1733388>, 2020.

1067 Yamamoto, S., Alcauskas, J. B., and Crozier, T. E.: Solubility of Methane in Distilled Water and
1068 Seawater, *J Chem Eng Data*, 21, 78–80, <https://doi.org/10.1021/je60068a029>, 1976.

1069 Zander, F., Heimovaara, T., and Gebert, J.: Spatial variability of organic matter degradability in tidal
1070 Elbe sediments, *J Soils Sediments*, 20, 2573–2587, <https://doi.org/10.1007/s11368-020-02569-4>,
1071 2020.

1072 Zander, F., Groengroeft, A., Eschenbach, A., Heimovaara, T. J., and Gebert, J.: Organic matter pools
1073 in sediments of the tidal Elbe river, *Limnologica*, 96, 125997,
1074 <https://doi.org/10.1016/j.limno.2022.125997>, 2022.

1075
1076
1077
1078
1079
1080
1081